The Salt Lake regional Smoke, Ozone and Aerosol Study (SAMOZA)

Final Report, September 29, 2023

Principal Investigators: Daniel Jaffe (UW), Lu Hu (UMt) and Seth Lyman (USU)

Executive summary

The Salt Lake City region is one of approximately 50 metropolitan regions around the U.S. that do not meet the 2015 8-hour ozone (O_3) National Ambient Air Quality Standard (NAAQS). To better understand the causes of high O_3 days in the region, a group of scientists from the University of Washington, Utah State University and the University of Montana developed and proposed the Salt Lake regional Smoke, Ozone and Aerosol Study (SAMOZA). The primary goals of SAMOZA are:

1. Make observations of a suite of VOCs, including many oxygenated VOCs by Proton Transfer Reaction Mass Spectrometry (PTR-MS) and the 2,4-dinitrophenylhydrazine (DNPH) cartridge method.
2. Evaluate whether UDAQ O_3 measurements show a positive bias during smoke events.
3. Quantify the range of concentrations of NO_x, VOCs, CO and $PM_{2.5}$ on smoke-influenced vs non-smoke days.
4. Conduct photochemical modeling and statistical modeling/machine learning analyses to improve our understanding of the sources of O_3 and $PM_{2.5}$ photochemistry (NOx vs VOC sensitivity) on both smoke-influenced and non-smoke days during the summer of 2022.

Key results:

i. We found no significant difference in the O_3 measurements from the "scrubber-less" UV instrument compared to the standard O_3 measurements made by UDAQ with a Teledyne T400 instrument at $PM_{2.5}$ concentrations up to 60 μg m^{-3}.

ii. For formaldehyde (CH_2O), which was measured by two different methods, there is a generally good correlation in the data from the two methods, but the PTR-MS measurements are approximately 50% greater than the DNPH measurements on smoky days. The cause for this difference is not yet known.

iii. On days with smoke, we found that $PM_{2.5}$, CO, O_3 and nearly all VOCs were significantly enhanced. On average, NO_x was also enhanced on days with smoke, but this was complicated by day of week effects on NOx concentrations (higher on weekdays).

iv. Photochemical modeling of O_3 production rates at the Utah Tech Center for both smoke influenced and no smoke days demonstrates a strong sensitivity to VOC concentrations and less sensitivity to NO_x. For non-smoke days, reductions in VOCs of ~30% result in significantly reduced O_3 production. Reductions in NO_x of ~60% are needed to get a significant reduction in O_3 production for non-smoke days.

v. The photochemical modeling shows that formaldehyde and other oxygenated VOC, along with alkenes, were the most important O_3 precursors.

vi. Generalized Additive Modeling (GAM) gave similar MDA8 O_3 enhancements on smoky days as the photochemical modeling. Analysis of the GAM results show that 19-31% of the smoke days have GAM residuals that exceed the EPA (2015) criteria for statistical analysis of O_3 data, and thus this method could be used as support for exceptional event cases for those days.

Introduction

Surface ozone (O_3) is formed from photochemical reactions of nitrogen oxides (NO_x = NO + NO_2) and volatile organic compounds (VOCs). O_3 has serious health impacts up to and including premature mortality (Bell et al., 2004; Di et al., 2017). The Northern Wasatch Front/Salt Lake City metropolitan region is one of approximately 50 regions in the U.S. that are considered non-attainment areas (NAAs) for the 2015 O_3 standard (https://www.epa.gov/air-trends/air-quality-design-values). The National Ambient Air Quality Standard (or NAAQS) for O_3 is currently 70 ppb and is based on the three-year mean of the annual fourth highest, maximum daily 8-hour average (MDA8) O_3 concentration.

In the Western U.S. there are several important challenges to meeting the standard. First background O_3, defined here as the distribution of concentrations that are observed in rural areas of the western U.S., is high due to the combined influences of stratospheric intrusions, a deep mixed layer and increasing area of wildfires burned each year (Jaffe et al 2018; 2020). Observations and models suggest that Nevada and Utah have some of the highest concentrations of background O_3 in the U.S. with a much larger contribution from the stratosphere compared to long distance anthropogenic sources (Langford et al 2017; Mathur et al 2022). In addition to these sources, wildfires emit O_3 precursors and can have substantial impacts on surface O_3 concentrations (Gong et al 2017; Buysse et al 2019; McClure and Jaffe-2018; Jaffe et al 2018; 2022; Rickly et al 2023; Permar et al 2023).

Specifically for the Northern Wasatch Front/Salt Lake City (SLC) region, concentrations of nitrogen oxides have been declining for the last decade, but the fourth highest O_3 MDA8 has been essentially stagnant over this time. In a study of national O_3 trends at 40 U.S. non-attainment areas, Jaffe et al (2022) found two things that were somewhat unusual for the SLC region. First, the relationship between annual fourth highest MDA8 O_3 and annual mean NO_2 was amongst the weakest of any of the sites considered. Second, while NO_2 concentrations have declined and displayed the typical pattern of higher values on weekdays, the pattern of enhanced O_3 remains relatively insensitive to the day of week. Similar relationships were also seen at other western U.S. sites and these patterns were attributed to the interannual variations in the influence from wildfires and stratospheric intrusions. At the same time, it is important to recognize that local emission sources also impact O_3 and, absent emissions from human and industrial sources, O_3 concentrations would rarely exceed the NAAQS levels (Jaffe et al 2020).

Project goals

Given this background, a group of principal investigators from the University of Washington (UW), Utah State University (USU) and the University of Montana (UMt) developed the SAMOZA plan. The over-arching goal of SAMOZA is to improve our understanding of O_3 and $PM_{2.5}$ in the SLC region during summer. Specific goals are:

1. Make observations of a suite of VOCs, including many oxygenated VOCs by Proton Transfer Reaction Mass Spectrometry (PTR-MS) and the 2,4-dinitrophenylhydrazine (DNPH) cartridge method.
2. Evaluate whether UDAQ O_3 measurements show a positive bias during smoke events.
3. Quantify the range of concentrations of NO_x, VOCs, CO and $PM_{2.5}$ on smoke-influenced vs non-smoke days.
4. Conduct photochemical modeling and statistical modeling/machine learning analyses to improve our understanding of the sources of O_3 and $PM_{2.5}$ photochemistry (NOx vs VOC sensitivity) on both smoke-influenced and non-smoke days during the summer of 2022.

Long-term context

Figure 1 shows the long-term pattern of O_3 and NO_2 at the Hawthorne monitoring site near downtown SLC. Figure 2 shows the same O_3 data along with the number of "smoke days" in each year. Smoke days are defined as days with satellite observed overhead smoke (from the NOAA HMS product (Rolph et al 2009; Kaulfus et al 2017) and surface $PM_{2.5}$ greater than the mean+1 SD of days with no overhead HMS smoke. The mean and SD for surface $PM_{2.5}$ with no overhead smoke is calculated from the daily mean values for May-Sept for each individual year.

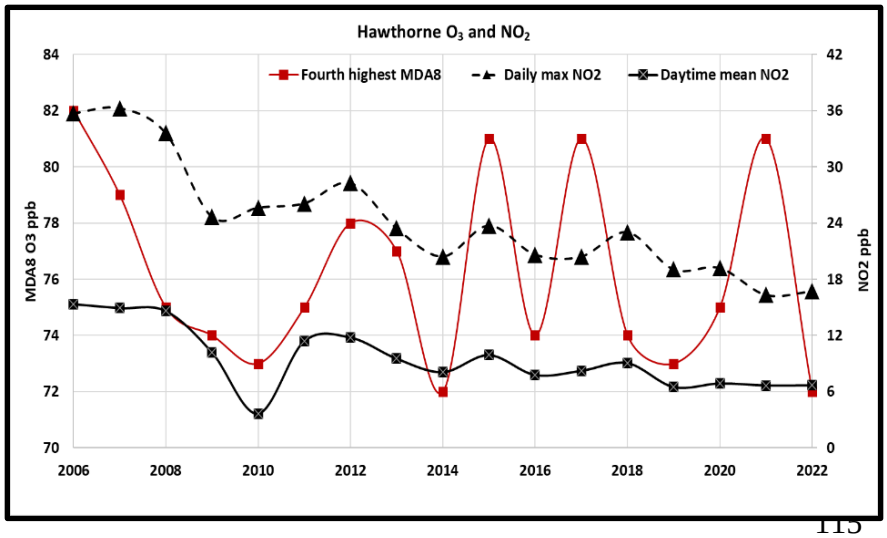

Figure 1. Annual fourth highest MDA8 O_3 and average May-September daily 1-hour maximum NO_2 and daytime mean NO_2 (0700-1400 local standard time) for the Hawthorne monitoring site.

115

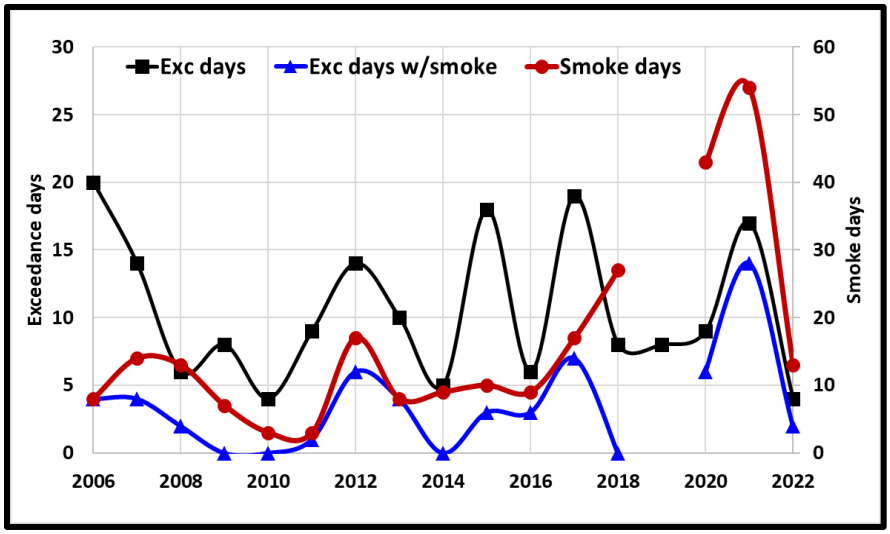

Figure 2. Number of O_3 exceedance days (MDA8>70 ppb) each year at Hawthorne site (left axis) number of exceedance days with smoke (left axis) and number of smoke days each year (right axis).

131

132

133 Figure 2 suggests that in some years, such as 2021 and possibly 2017, strong influence from
134 smoke likely enhanced O_3 and contributed to the elevated fourth highest MDA8 in those years.
135 The SAMOZA experimental period (summer 2022), appears to have taken place during a
136 relatively lower fourth highest MDA8 O_3 value (72 ppb) and number of smoke days (13 days),
137 compared to the past decade (76 ppb and 18 days, respectively). At Hawthorne, there were 4
138 exceedance days in 2022, two of which had smoke, while at the UTC site, there were 6
139 exceedance days in 2022.

140

Methods

Measurements for the SAMOZA study were conducted from August 1-October 1, 2023 at the Utah Department of Environmental Quality Technical Support Center (hereafter simply UTC), located approximately four miles east of the Salt Lake City International Airport at 40.78°, -111.94°. This site was chosen due to available space and power, along with the fact that other key observations were already being made there. The SAMOZA measurements included the following:

a. O_3 using a scrubber-less UV instrument (2B Technologies, Model 211).

In addition to the standard UDAQ measurements of O_3 at UTC, the SAMOZA team measured ambient O_3 concentrations using a 2B Technologies Model 211 O_3 monitor (Boulder, CO), a dual-beamed 254 nm photometer at 1-minute resolution. This instrument uses the reaction between ambient O_3 and NO generated in situ by upstream photolysis of added nitrous oxide (N_2O) to quantify ozone by UV photometry without the issues affecting conventional O_3 scrubbers. The instrument was calibrated daily during the campaign against a reference photometer (2B Technologies model 306) that was itself cross referenced to an O_3 standard from the NOAA Global Monitoring Lab (Birks, et al. 2018). The O_3 monitor (and the CO instrument) shared the same sampling line as the PTR-MS described below. Resolution of the O_3 monitor is 0.1 ppb, with a limit of detection (2σ) of 1.0 ppb for a 10 s average.

b. Proton Transfer Reaction Mass Spectrometric (PTR-MS) measurements of Volatile Organic Compounds (VOCs).

Ambient VOCs were measured using proton-transfer-reaction time-of-flight mass spectrometry (PTR-ToF-MS 4000, Ionicon Analytik GmbH, Innsbruck, Austria). The conditions in the drift tube were held constant during the campaign at 3.00 mbar, 60°C, and 815V, which made for an electric field of 135 Td. The PTR-MS was located on the second floor of the Technical Support Center. The sampling inlet was made from perfluoroalkoxy (PFA) tubing and was situated on the roof of the building, ~20m above ground level. The air was subsampled by the PTR-MS through ~100 cm of 1/16" (1.59 mm) OD polyetheretherketone (PEEK) tubing maintained at 60°C. Ions from m/z 19 to 400 were measured once every minute. Instrument background was taken approximately every 2½ hours by measuring VOC-free air generated by ambient air passing through a heated catalytic converter (375°C, platinum beads, 1wt% Pt: Sigma Aldrich).

Calibrations were performed for 25 species in two compressed gas standard cylinders (stated accuracy 5% at ~1 ppmv; Apel-Riemer Environmental, Inc., Miami, FL; Permar et al., 2021). One cylinder with 10 species was used every other day for the duration of the campaign and was calibrated via dynamic dilution followed by addition of gas to the VOC-free air described above. A second standard gas cylinder containing 15 species was used every other day for the first three weeks of the campaign. Six-point calibrations were performed between 1 and 7 ppb. Only those calibrations with an R^2 above 0.998 and with sensitivities for the same species within 10% during the campaign were used. From quadrature addition of individual errors including calibration and mass flow controllers in the instrument, uncertainty for these species is <15%. In addition, D5 Siloxane was calibrated with a gas standard in June 2022 before the campaign (stated accuracy 5% at ~1ppm; Apel-Riemer Environmental, Inc., Miami, FL) using dilution as described above. Uncertainty for this species is <15%.

Formaldehyde was calibrated after the campaign using a gas standard in a compressed cylinder (stated accuracy 5% at ~2ppmv; Airgas USA LLC, Plumsteadville, PA) diluted with a zero-air generator (7000 Zero Air Generator, Environics, Tolland, Connecticut). Gases were mixed in a Liquid Calibration Unit (Ionicon Analytik GmbH, Innsbruck, Austria) and water was introduced to find the dependence of sensitivity on changing humidity. Formic acid and acetic acid were calibrated before the campaign using liquid standards evaporated and diluted with zero-air in the same Liquid Calibration Unit. Water vapor was used to find humidity dependence of sensitivity as described above. Uncertainty for these species is estimated at 40%, with the major source of error being instrument drift over time.

Sensitivity for maleic anhydride was estimated using the method by Sekimoto et al. (2017) from its molecular dipole moment and polarizability. The procedure for the calculation was further refined in a previous work (Permar et al., 2021). The uncertainty for this species is estimated to be 50%.

Mass spectra were first analyzed with Ionicon's PTR-Viewer software (Version 3.4, Ionicon Analytik). One-minute mass calibrations performed during the campaign were refined using 4 ion peaks: m/z 29.9974 [NO^+], 59.0491 [$C_3H_6OH^+$], 203.943 [$C_6H_4IH^+$], and 330.848 [$C_6H_4I_2H^+$]. Ion masses were assigned molecular formulae using a peak list included with the software which was compared and adjusted according to a library of previously published PTR-MS mass peaks (Pagonis et al., 2019). Ion counts for each peak in the list were calculated by the

PTR-Viewer software through a baseline correction as well as a correction for mass discrimination in the time-of-flight. The calculated ion counts were then exported for further processing in R. Instrument background was linearly interpolated and subtracted from the data. Each ion was normalized to the primary ion [H_3O^+] and water cluster ion [$(H_2O)H_3O^+$]. Normalized counts were converted to mixing ratios using the sensitivities found during calibration.

c. DNPH measurements of carbonyl species

We collected carbonyl samples by pulling ambient air through 2,4-dinitrophenylhydrazine (DNPH) cartridges (Waters WAT037500) with potassium iodide cartridges (WAT054420) upstream to remove ozone. The sample path upstream of the cartridges was composed entirely of PFA and PTFE Teflon, with a PTFE filter (5 μm pore) upstream of the sample line to filter particles (5 μm pore size). The DNPH cartridges were installed in automatic sampling trays with solenoid valves to control flow through each cartridge. A pump provided flow, and a mass flow meter measured the flow rate. Flow through cartridges was about 1 L min^{-1}. A Campbell Scientific CR1000 data logger controlled the system and recorded sample flow rates. We collected three 3-h DNPH samples per day from 1 August 2023 through 3 October 2023. Daily sampling times were 9:30-12:30, 12:30-15:30, and 22:30-0:30 local standard time. We replaced the DNPH cartridges in the sampling trays weekly. After sampling, the cartridges were kept refrigerated storage and transport. One pair of samples was collected simultaneously on two different trays each week as a duplicate. Field blanks were collected weekly by installing DNPH cartridges in a sampling tray and immediately removing them.

We eluted cartridges within 14 days of sampling and analyzed the eluent within 30 days. To elute DNPH cartridge samples, we flushed cartridges with 5 mL of a solution of 75% acetonitrile and 25% dimethyl sulfoxide (percent by volume). We collected the solution into 5 mL volumetric flasks and brought the flasks to a volume of 5 mL using 0.5–1 mL of the acetonitrile/dimethyl sulfoxide solution. Finally, we pipetted a 1.6 mL aliquot from the 5 mL flask into two 2 mL autosampler vials for analysis by high-performance liquid chromatography (HPLC). The second vial was kept as a spare in case of contamination or equipment failure.

We used a commercial standard mixture (M-1004; AccuStandard) of derivatized carbonyls in acetonitrile for calibration. We analyzed samples with a Shimadzu Nexera-i LC-2040C 3d Plus HPLC and a Shimadzu Shim-Pack Velox C18 column. We used a mixture of acetonitrile,

tetrahydrofuran, and water as the eluent. We calibrated the instrument on each analysis day with a 5-point calibration curve. We ran at least 1 additional calibration standard at the beginning and end of each analysis batch to check for retention time drift or other errors. Target compounds analyzed are formaldehyde, acetaldehyde, acetone, acrolein, propionaldehyde, crotonaldehyde, 2-butanone, methacrolein, n-butyraldehyde, valeraldehyde, m-tolualdehyde, and hexaldehyde. More information about the methods used is available in Lyman et al. (2021).

Compounds in the laboratory blanks were 0.1 ± 0.1 ppb (average ± 95% confidence interval), and field blanks were 0.2 ± 0.2 ppbv in air. (The average volume of air sampled by field samples was applied to blank samples to convert blank results to units of ppbv in ambient air.) All samples were blank-corrected. Compounds in duplicate samples were 20 ± 5% different. Calibration recovery was 103 ± 2%. Detection limits 0.1 to 0.2 ppb.

We also received three DNPH cartridges loaded with carbonyls from Eastern Research Group (ERG), an independent laboratory that performs DNPH cartridge analysis for the U.S. Environmental Protection Agency and others. Excluding crotonaldehyde, our analytical results were 14 ± 4% higher than the results from ERG. Our crotonaldehyde results were 105 ± 30% higher, perhaps indicating an error in peak integration for crotonaldehyde.

d. CO using a gas chromatography (GC) with a reducing compound photometer

In addition to the standard UDAQ measurements of CO at UTC, the SAMOZA team made cconcurrent CO measurements using chromatography (GC) with a reducing compound photometer (Peak Performer 1; Peak Laboratories LLC., USA). CO eluting from the GC column pass directly into a heated mercuric oxide bed, resulting in liberated mercury vapor, which is subsequently measured via UV light absorption in the photometer cell. Compressed ultra-high purity air was used as the carrier gas. Multi-point calibrations are carried out before and after the campaign by dilution of a ppmv-level standard (Scott Specialty Gases, USA; stated accuracy ±2 %) into UHP air. The detection limit for CO is 300 pptv and the time resolution of the data was 3-minutes.

Meteorology, NO_x and $PM_{2.5}$ data were collected by the Utah Department of Environmental Quality at the UTC site and these were used in our analysis.

Models.

In addition to these observations several other modeling tools were used including the FOAM box model (Wolfe et al 2016; Ninneman and Jaffe 2021), a machine learning/statistical modeling (Gong et al 2017) and Positive Matrix Factorization. Each of these will be described along with the specific results in the results section below.

Results

Overview

Meteorological data were collected at the measurement site by the Utah Department of Environmental Quality. Relative humidity and ambient temperature were measured simultaneously with an electronic thin film air temperature and relative humidity sensor. Wind direction and speed were measured with 2D-ultrasonic anemometer transducers. All meteorological instruments were situated on a tower on the UDEQ building at the UTC. During the SAMOZA campaign, daily maximum temperatures (DMT) averaged 30.8°±4.8^{o}C (mean ± standard deviation). Temperatures were warmer for the first part of the campaign through September 8th (mean DMT of 33.3^{o}C) when temperatures started to cool down for the remainder of the campaign (mean DMT of 26.4^{o}C). Winds came mostly from the southeast, with some influence from the northwest. The highest wind speed seen was 19m/s, while the average was around 6 m/s.

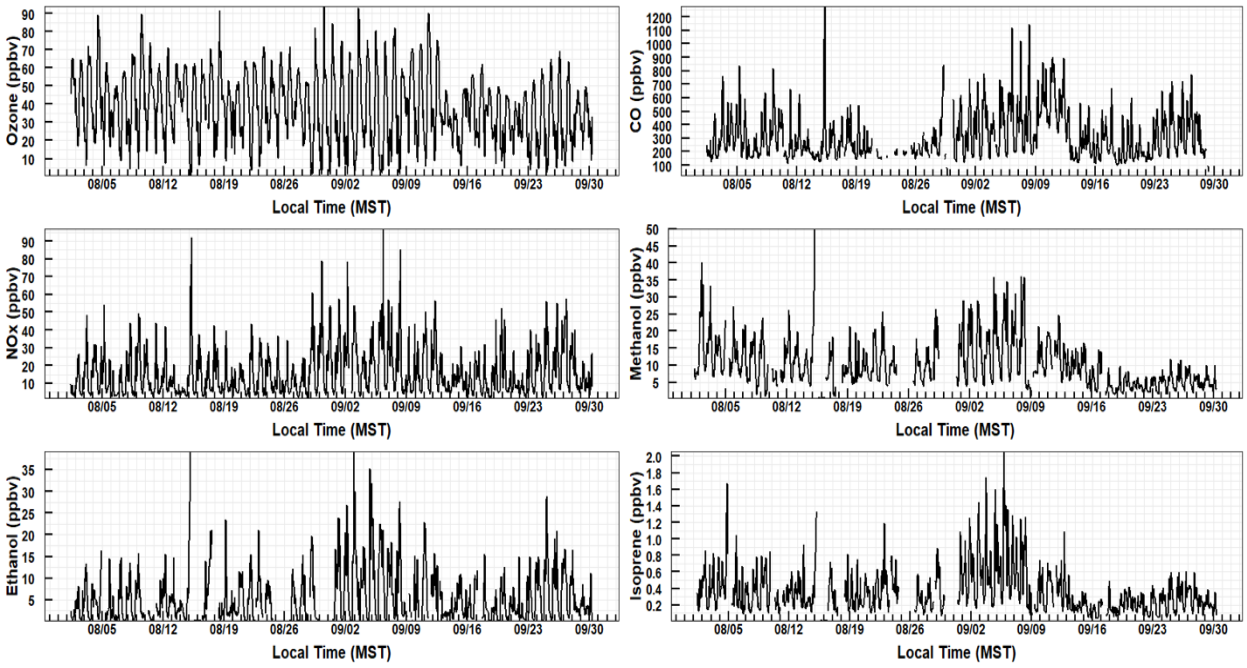

Figure 3. Time series of selected trace gas concentrations measured at the UTC site during the SAMOZA campaign (8/1/2022-9/30/2022).

As mentioned above, the summer of 2022 was a relatively modest year for smoke, with only about 10 days with identified smoke. At the UTC site there were 6 exceedances days (MDA8>70 ppb), five of which occurred during the SAMOZA experimental period (Aug.-Sept. 2022. Two of these exceedance days were associated with smoke (9/7/22 and 9/11/22). Four of the smokiest days were Sept. 9-12, 2022, with the highest daily mean $PM_{2.5}$ values observed on Sept. 10^{th} (33.8 µg m^{-3}). Sept 11^{th} also had smoke, with a daily mean $PM_{2.5}$ value of 25.3 µg m^{-3} and an O_3 MDA8 of 80 ppb. During this time, smoke covered a large portion of the western U.S., with large fires burning in Idaho, Oregon, Washington and California.

We use the NOAA Hazard Mapping System-Fire and Smoke Product (hereafter simply HMS) as an indicator of overhead smoke (https://www.ospo.noaa.gov/Products/land/hms.html). This satellite product provides mapping of fire locations and smoke extent for North America on a daily basis. However, as many have pointed out (e.g., Kaulfus et al., 2017, etc.), the smoke extent maps are indicative of overhead smoke and not necessarily of surface smoke. Figure 4 shows the hourly distribution of $PM_{2.5}$ at UTC for August-September of 2022, binned by daily HMS smoke detections, where HMS=0 indicates no overhead smoke and HMS=1 indicates overhead smoke detected. The standard deviation (SD) within each hourly bin is only shown for the HMS=0 data. The SDs within each hour for the HMS=1 data are larger, in the range of 9-13

304 µg m^{-3}. The overall means (using the daily average data) for the HMS=0 and 1 data are 6.2 and
305 11.9 µg m^{-3} and there were 42 and 19 days in each category, respectively.
306 Binning the data by only the HMS status will include some time periods with overhead
307 smoke, but minimal influence at the surface. For this reason, we add a $PM_{2.5}$ criteria to identify
308 "smoke days" at the surface. For this we use the mean (6.23 µg m^{-3}) and 1 SD (1.85 µg m^{-3}) of
309 the $PM_{2.5}$ concentrations on HMS=0 days, such that smoke days are defined as those with
310 HMS=1 and the daily mean $PM_{2.5}$ > 8.1 µg m^{-3}. For August-September 2022, there were 10 days
311 that met the criteria as a "smoke day" and 51 that were deemed a "no-smoke day". Figure 5
312 shows the diurnal pattern of $PM_{2.5}$ data binned by the smoke day criteria and Table 1 shows a
313 summary of the SAMOZA data binned by the smoke/no smoke categories.
314 There are several duplicate measurements. CO was measured using both the standard
315 UDAQ instrument as well as one provided by SAMOZA. While the agreement between these
316 two measurements is good (the correlation coefficient of hourly data is 0.86), we do see that the
317 SAMOZA data are biased high compared to the UDAQ measurements, as evidenced by both the
318 mean values (see Table 1) and the correlation slope of 1.15 (SAMOZA CO vs UDAQ CO).
319 Given that this has little policy implication, we do not investigate the cause of this bias further.
320

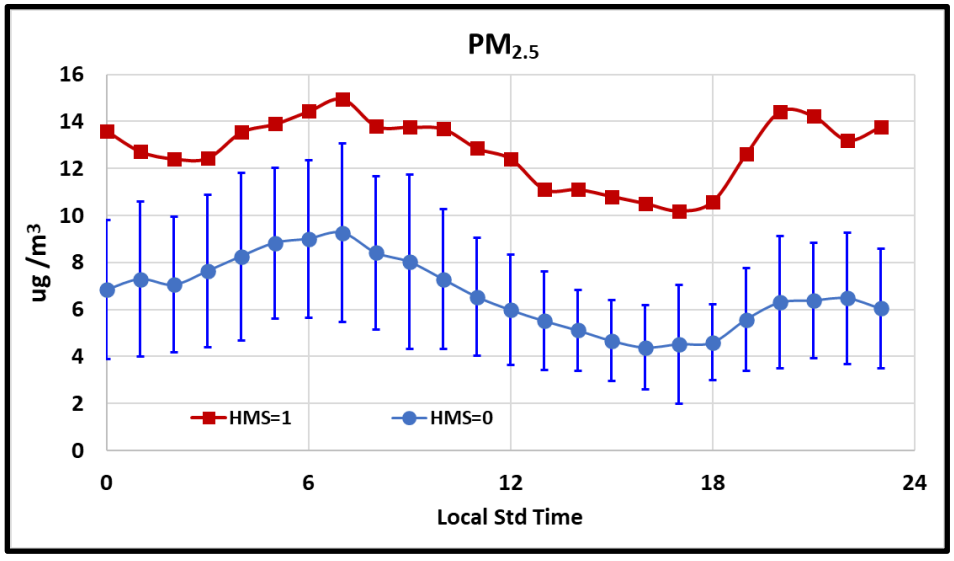

Figure 4. $PM_{2.5}$ measured at UTC in August-September 2022, binned by HMS smoke detections. Errors bars are 1 standard deviation and are only shown on the HMS=0 data for clarity. This includes 19 days with HMS=1.

336

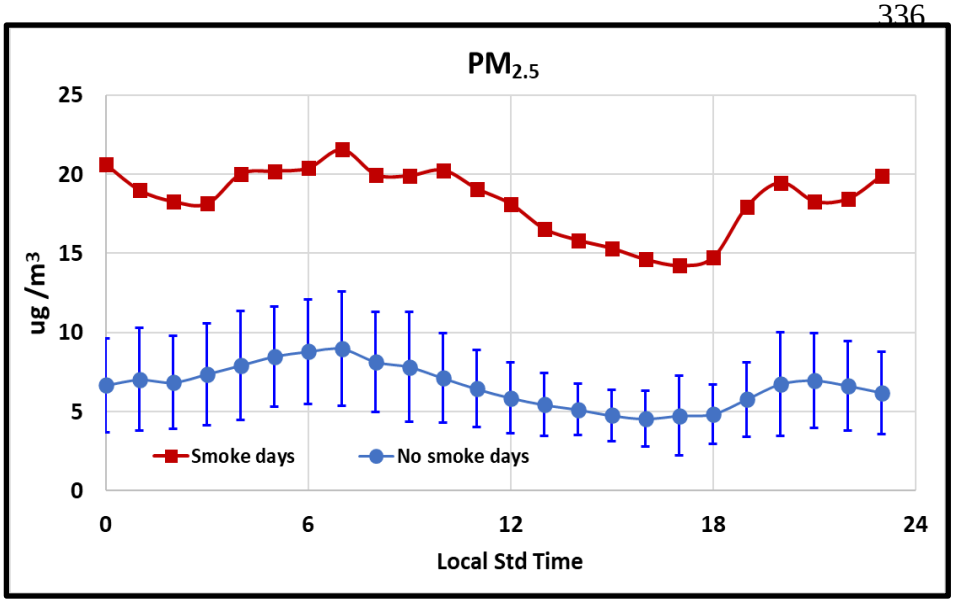

Figure 5. $PM_{2.5}$ measured at UTC in August-September 2022, binned by "smoke day" criteria (mean+1 SD of daily mean $PM_{2.5}$ on HMS=0 days). Errors bars are 1 standard deviation and are only shown for the no smoke data. This includes 10 days identified as "smoke days"

353

354

Table 1. Summary of data during the SAMOZA experiment (August-September, 2022). All data are in ppb except $PM_{2.5}$ (µg/m3) and ∑VOCs as C (ppbC).

	Daily $PM_{2.5}$	MDA8 O_3[a]	CO[a]	CO[b]	O_3[a]	O_3[b]	NO_x
All data	8.0	56.9	182	314	37.4	38.7	15.8
No smoke (n=51 days)	6.2	55.4	160	284	37.0	38.2	15.0
Smoke days (n=10 days)	17.3	65.0	293	446	39.4	41.1	20.5
	Formal-dehyde[c]	**Ace-tone[c]**	**Iso-prene[c]**	**∑VOCs[d]**	**∑VOCs as C (ppbC)[d]**	**Formal-dehyde[e]**	**Ace-tone[e]**
All data	4.3	3.4	0.4	15.6	37.9	3.6	4.0
No smoke (n=51 days)	3.7	3.2	0.3	14.2	34.6	3.4	3.8
Smoke days (n=10 days)	7.1	4.4	0.5	22.1	53.2	4.6	5.0

[a]This column reports data from the UDAQ instrument.
[b]This column reports data from the SAMOZA instrument.
[c]Data from PTRMS instrument.
[d]This includes these VOCs as reported by the PTRMS instrument (Formaldehyde, Propyne, Acetonitrile, Acetaldehyde, Formic Acid, Butenes, Acetone, Isoprene, MVK_MACR, MEK, Benzene and Toluene. See PTRMS dataset for full list of compounds measured.
[e]Data from DNPH cartridge method.

Next we can examine the diurnal cycle of various pollutants as a function of smoke/non-smoke status. Figure 6 shows the average diurnal cycle for CO, O_3, formaldehyde, NOx, ∑VOCs and ∑VOCs as ppbC.

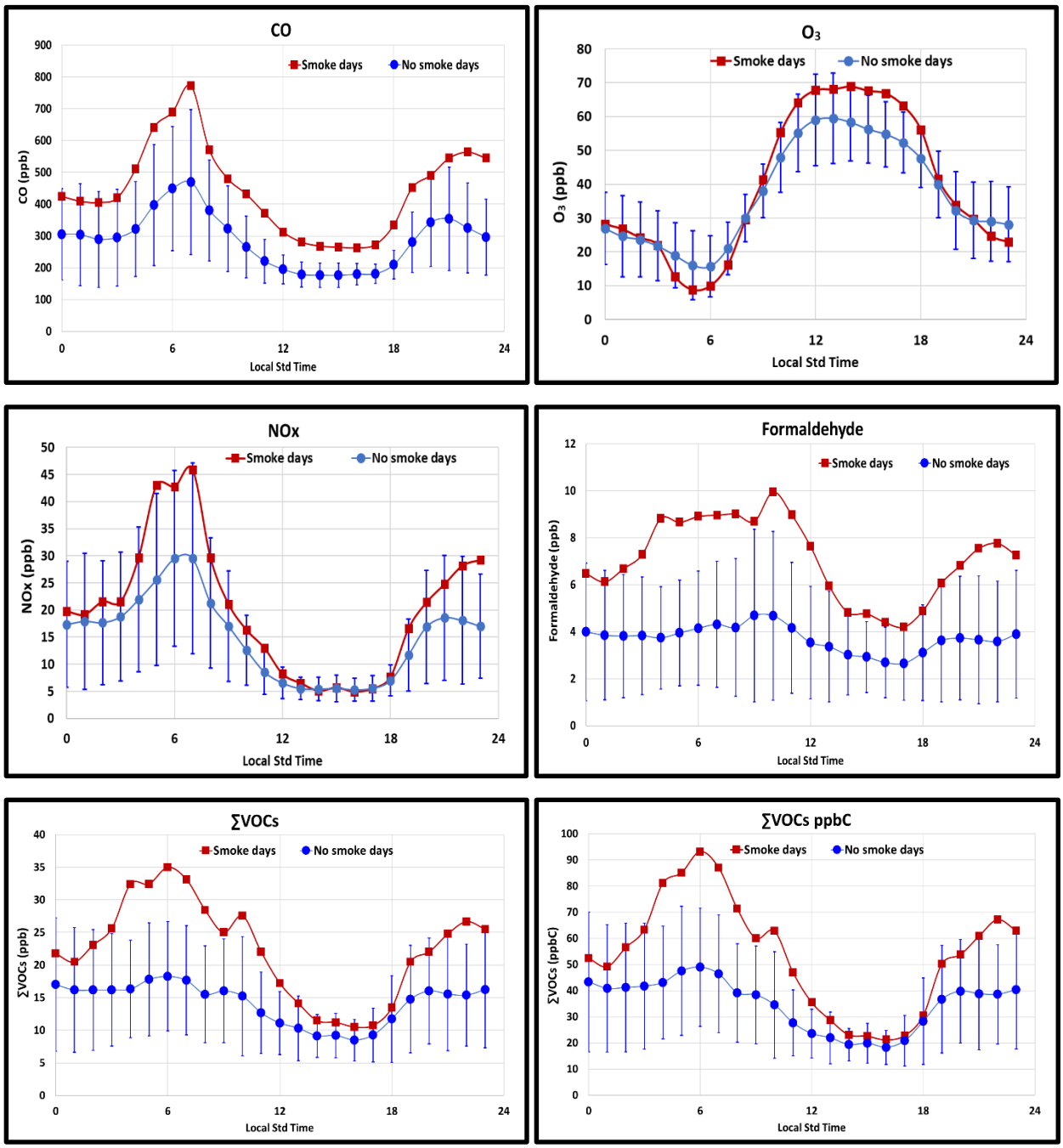

Figure 6: Diurnal cycles of CO, O_3, formaldehyde, NOx, ∑VOCs (ppb) and ∑VOCs (as ppbC). Error bars show one standard deviation on the no smoke data.

In general, the smoke/non-smoke patterns are consistent with previous work (e.g. Buysse et al 2017; Ninneman and Jaffe 2021). Some of the key patterns are:

1. O_3 increases more rapidly during the morning hours and reaches higher peak values for smoky conditions compared to non-smoky conditions.

2. CO, $PM_{2.5}$ and VOCs are all significantly elevated on smoky days, compared to non-smoky days.
3. Emissions from traffic are seen on all days, as evidenced by rapid increases in CO, NOx and VOCs in early morning hours.

The most surprising result is that NO_x concentrations appear to be greater on smoky days, which differs slightly from previous work. Buysse et al (2019) found that NO_x was enhanced on some days at some locations during smoke, but not at other locations. We found that NO_x was higher on average, but the pattern is not very robust, given the high variability in NO_x concentrations. Figure 7 compares the NO_x diurnal cycle on two smoke days with data from all nonsmoke days.

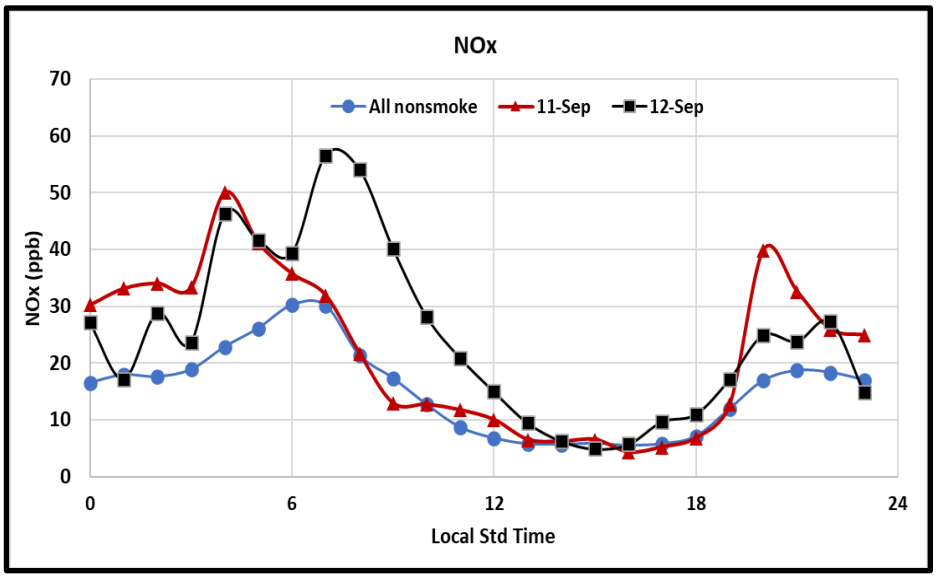

Figure 7: Average diurnal cycle for NO_x for all non-smoky days and the diurnal pattern for September 11th and 12th, 2022. The MDA8 O_3 values were 80 and 68 ppb for September 11th and 12th, respectively.

We note that Sept. 11th was a Sunday, and while there was a surprising level of NO_x overnight, by morning the levels had returned to typical values for a non-smoky day. In contrast, Sept. 12th, a Monday, had very high NO_x levels which persisted until past noon. The pattern of O_3 on these two days is counter to the NO_x values, with a higher MDA8 on Sunday the 11th (80 ppb), compared to Monday the 12th (68 ppb), suggesting that the high NO_x levels on the 12th, may have suppressed O_3 formation. Figure 8 shows the diurnal pattern for all non-smoky days vs day of week. A clear pattern is evident with highest NO_x concentrations on Monday and Tuesday and lowest values on Saturday and Sunday.

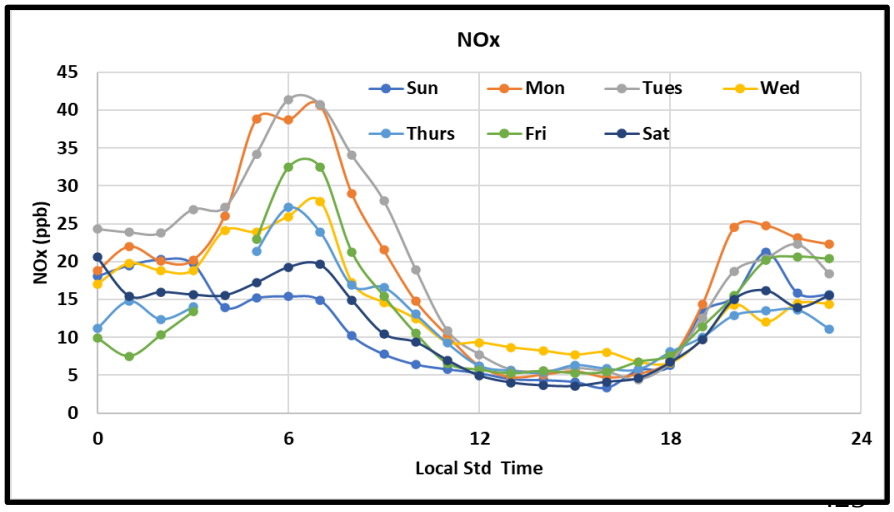

Figure 8: Mean diurnal cycle for NO_x for all non-smoky days.

Table 2 shows the data sorted by exceedance status. An exceedance day is one with an MDA8>70 ppb.

Table 2. Mean values for all days and exceedance days by smoke/no-smoke status for Aug.-Sept. 2022.

	No-smoke	Smoke
ALL STUDY DAYS		
Count (days)	51	10
Average MDA8 (ppb)	55.3	65.0
Average NOx (ppb)	15.0	20.5
Average ∑VOCs (ppb)	14.2	22.1
Average PM25 (µg/m^3)	6.1	17.3
O_3 EXCEEDANCE DAYS		
Count (days)	3	2
Average MDA8 (ppb)	76.0	75.5
Average NOx (ppb)	20	22.6
Average ∑VOCs (ppb)	23.1	26.8
Average daily PM25 (µg/m^3)	8.5	17.8

Binning the data this way shows that both NO_x and VOCs are, on average, enhanced on exceedance days by 33 and 63%, respectively, for non-smoke days.

435 **Comparison of O_3 measurements by standard UV and scrubber-less UV**

436 Because previous work has shown that some UV O_3 instruments can exhibit significant
437 positive biases in smoke (e.g. Long et al 2021; Bernays et al 2022), one of the SAMOZA goals
438 was to compare the standard UV O_3 measurements (made with a Teledyne T400 instrument)
439 with a scrubber-less UV that has previously been shown to have little to no bias in smoke (Long
440 et al 2021). Figure 8 shows a comparison of hourly averages measured with the two instruments
441 at UTC and Figures 9 and show the difference in the two observations as a function of $PM_{2.5}$
442 (Figure 9) and CO (Figure 10).
443

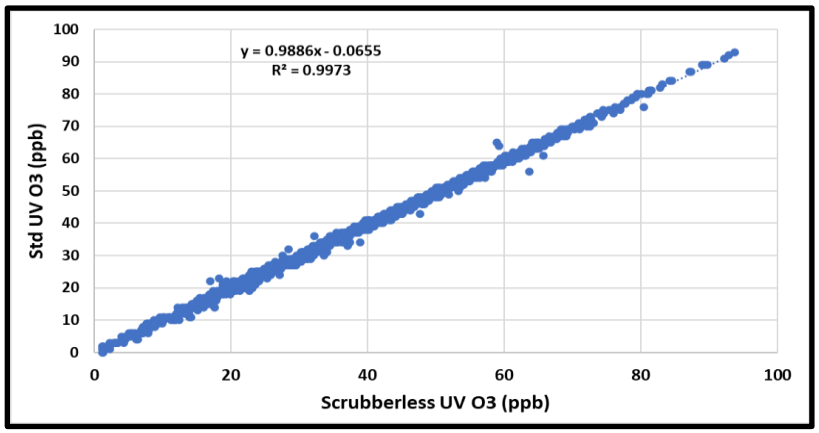

Figure 8. Comparison of the hourly data from the standard UDAQ Teledyne T400 instrument with the SAMOZA observations using a TwoB Technologies model 211 scrubber-less instrument.

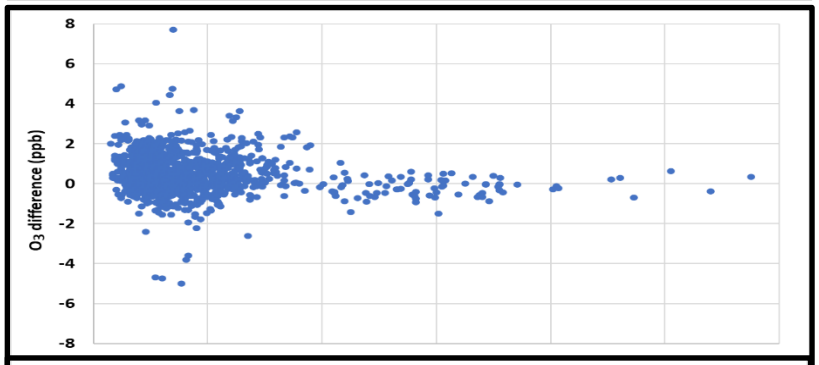

Figure 9. Difference between the two O_3 measurements as a function of $PM_{2.5}$ concentrations.

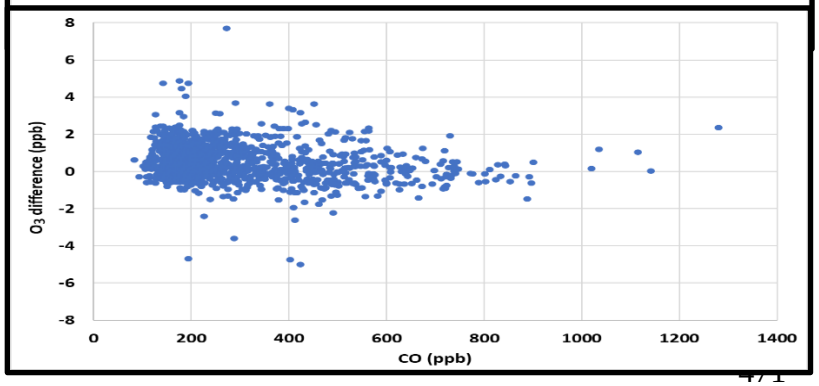

Figure 10. Difference between the two O_3 measurements as a function of CO concentrations.

During SAMOZA, moderate smoke impacted the region on a number of days, with the highest hourly $PM_{2.5}$ value of 58 µg m^{-3} on Sept. 10th, 2022. As seen in Figures 7, 8 and 9, this level of smoke causes no detectable bias in the standard UV measurements at UTC. Long et al (2021) reports the O_3 bias for several standard UV instruments in terms of ppb of bias per ppm of CO in smoke. Generally the bias for instruments that include an internal drying system was found to be much smaller then instruments without a drying system. For the "undried" instruments the observed bias was 16.5-24.0 ppb per ppm of CO, compared to 1-3 ppb per ppm of CO for the systems with drying. Given the observations during SAMOZA, and despite having only moderate smoke levels, we can conclude that a bias of this magnitude would have been observable. So based on the SAMOZA results, we see no significant bias in smoke with the standard UDAQ O_3 measurements up to at least 1 ppm of CO.

Photochemical box modeling

Numerous studies have demonstrated that photochemical box models are useful tools for investigating O_3 formation in smoke plumes (e.g., Mason et al., 2006; Alvarado et al., 2015; Müller et al., 2016; Coggon et al., 2019; Ninneman and Jaffe, 2021; Rickly et al., 2023). Critical to the success of these studies was their ability to include observations of the key chemical species in the model and use a chemical mechanism that sufficiently accounted for the complex chemistry that occurs in smoke plumes. In this section, we apply a photochemical box model, constrained to the observations, to examine the VOC and NO_x sensitivity on four high O_3 days in 2022.

The observed hourly NOx, speciated VOCs, pressure temperature and RH were used to constrain the Framework for 0-D Atmospheric Modeling (F0AM) photochemical box model (Wolfe et al., 2016). We used version 3.3.1 of the Master Chemical Mechanism (MCM v3.3.1; http://mcm.york.ac.uk) to drive the chemistry in the model (e.g. Jenkin et al., 2015). For each case study day, a three day simulation was completed to investigate photochemical O_3 production at UTC, where only the results from the third day were considered, to allow for model spin-up. The model used an integration time step of 10 minutes.

F0AM was constrained to the measured VOCs listed in Table 3. Total methylfurans were assumed to consist entirely of 2-methylfuran, consistent with Coggon et al. (2019). Since the PTR-MS only measured total concentrations of butenes, C8–C10 aromatics, and monoterpenes, the distribution among individual species was estimated using data collected at the SLC Hawthorne site. In addition, F0AM was constrained to observed total NO_x concentrations at

each time step, while the model chemistry determined the NO/NO_2 ratio. For all simulations, O_3 was unconstrained and initialized with the concentrations measured at 0:00 LST.

Table 3. List of VOCs used to constrain the model. The unitalicized parameters were measured at UTC by the PTR-MS. Speciation for the italicized parameters were estimated based on data from the Hawthorne sites, as described in Ninneman et al 2023.

VOC Class	Parameters
Aldehydes	Formaldehyde and acetaldehyde
Alkenes	Total butenes [a] (*1-butene*, *cis-2-butene*, *trans-2-butene*)
Aromatics	Benzene, toluene, total C8 aromatics [a] (*ethylbenzene*, *m-xylene*, *o-xylene*, *p-xylene*, *styrene*), total C9 aromatics [a] (*1,2,3-trimethylbenzene*, *1,2,4-trimethylbenzene*, *1,3,5-trimethylbenzene*, *isopropylbenzene*, *m-ethyltoluene*, *o-ethyltoluene*, *p-ethyltoluene*, *n-propylbenzene*), and total C10 aromatics [a] (*m-diethylbenzene*)
Alcohols	Methanol and ethanol
Ketones	Acetone, methyl vinyl ketone, and methyl ethyl ketone
Biogenic VOCs (BVOCs)	Isoprene and total monoterpenes [a] (*alpha-pinene*, *beta-pinene*)
Furans	Furan, total methylfurans (*2-methylfuran*), furfural, and methylfurfural
Other	Acetonitrile

On each case study day, we used the daily 25th-percentile concentration for odd oxygen ($O_x = NO_2 + O_3$) to prescribe fixed background O_3 concentrations in the model. Since UTC is a high-NO_x site, O_x was used instead of O_3 to determine background O_3 concentrations because O_x is unaffected by NO titration. The resulting daily 25th-percentile O_x values were 49.0, 42.8, 49.8, and 52.8 ppb on 4 August and 3, 11, and 12 September, respectively. These values are consistent with the relatively high background O_3 concentrations reported for many parts of the western U.S. (Jaffe et al 2020).

NO_2 photolysis rates (J_{NO2}) were estimated using an equation developed by Trebs et al. (2009):

$$J_{NO2} = (1 + \alpha) \times ((B_1 \times SR) + (B_2 \times SR^2)) \qquad (1)$$

where J_{NO2} has units of s^{-1}, α is the surface albedo, B_1 and B_2 are polynomial coefficients with values of $1.47 \times 10^{-5}\ W^{-1}\ m^2\ s^{-1}$ and $-4.84 \times 10^{-9}\ W^{-2}\ m^4\ s^{-1}$, respectively, and SR is the measured solar radiation in $W\ m^{-2}$. We assumed an α of 0.15, which is a typical value for an urban area. Photolysis rates for all other parameters were computed as a function of the

528 overhead O_3 column (300 DU), α (0.15), elevation of UTC (1286 m a.s.l.), and solar zenith angle
529 using model-provided lookup tables that are described elsewhere (Wolfe, 2020). Then, the
530 model-calculated photolysis rates were scaled in reference to the J_{NO2} values calculated from
531 equation 1. This was done to account for smoke impacts on photolysis for all species.
532 The heterogeneous uptake of hydroxyl radical (OH) and hydroperoxyl radical (HO_2) onto
533 aerosols was included based on previous studies (Tang et al., 2014;Lindsay et al., 2022):
534
535 $$dX / dt = -0.25 \times \gamma \times c(X) \times PM_{2.5} \times SA_{specific} \times X_g \times 10^{-6} \quad (2)$$
536
537 where dX / dt is the heterogeneous loss rate of OH or HO_2 in ppb s^{-1}, γ is the aerosol uptake
538 coefficient, c(X) is the average molecular speed of OH or HO_2 in m s^{-1}, $PM_{2.5}$ has units of μg
539 m^{-3}, $SA_{specific}$ is the specific aerosol surface area in m^2 g^{-1}, and X_g is the concentration of OH or
540 HO_2 in ppb that is in the gas phase. γ was assumed to be 0.2, following Jacob (2000) and Slade
541 and Knopf (2014). Molecular weight and temperature were used to determine c(X). $SA_{specific}$ was
542 assumed to be 4 m^2 g^{-1}, following Lindsay et al. (2022).
543 A first-order dilution rate (K_{dil}) was used to account for mixing of background O_3 into the
544 model domain. This was done by varying K_{dil} until the best fit between modeled and observed
545 afternoon O_3 was achieved, consistent with previous work (McDuffie et al., 2016; Ninneman et
546 al., 2020; Ninneman and Jaffe, 2021; Rickly et al., 2023). The K_{dil} values that led to the best fit
547 between modeled and measured afternoon O_3 on 4 August and 3, 11, and 12 September were 1.3
548 × 10^{-4}, 1.5 × 10^{-4}, 9.0 × 10^{-5}, and 1.6 × 10^{-4} s^{-1}, respectively.
549 Model calculated instantaneous O_3 production rates (P_{O3}) were used to investigate O_3
550 formation at UTC on the case study days. P_{O3} was calculated using eq. 3:
551
552 $$P_{O3} = k_{HO2+NO}[HO_2][NO] + \sum_i k_{RiO2+NO}[R_iO_2][NO] \quad (3)$$
553
554 where k_{HO2+NO} and $k_{RiO2+NO}$ are the rate constants for the reactions of HO_2 with NO and speciated
555 organic peroxy radicals (R_iO_2) with NO, respectively. Unlike the net O_3 production, P_{O3} does not
556 consider other processes that are important in the O_3 budget, including chemical loss, dry and
557 wet deposition, and advection. A series of model sensitivity tests were completed to examine the
558 impact of anthropogenic VOCs, NO_x, and/or temperature on P_{O3} and O_3 at UTC. Except for

isoprene and monoterpenes, all measured VOCs were considered to be anthropogenic. Many/most of the VOCs are also enhanced during wildfire smoke. For the sensitivity tests, we only varied the initial values for anthropogenic VOCs, NO_x, and/or temperature. The other model inputs were left unchanged.

Figure 11 and Table 4 show the key observations on the four case study days. MDA8 O_3 concentrations on three out of the four days – 4 August, 3 September, and 11 September – exceeded the O_3 standard of 70 ppb. Even though there was smoke overhead on 3 September, the 24 h $PM_{2.5}$ concentration was only 8.5 µg m^{-3}. As a result, we conclude that smoke negligibly impacted surface concentrations on 3 September. Hourly O_3 and $PM_{2.5}$ were uncorrelated on 11–12 September when morning O_3 concentrations rapidly increased from 15 to 84 ppb and 13 to 66 ppb on 11 and 12 September, respectively. This indicates that the observed O_3 was mainly due to in-situ photochemical production, rather than transport from the smoke plume. Figure 11, shows that the daytime median concentrations of ∑VOCs were similar on all four days, although there were higher aldehydes on Sept. 3rd, compared to other dates. NOx concentrations for three of the days were similar, but much higher on September 12th, a Monday. Conditions were favorable for O_3 production on the case study days, with daily maximum temperatures (T_{max}) exceeding 30 °C, although temperatures were warmer on August 3rd and September 4th, compared to the other days.

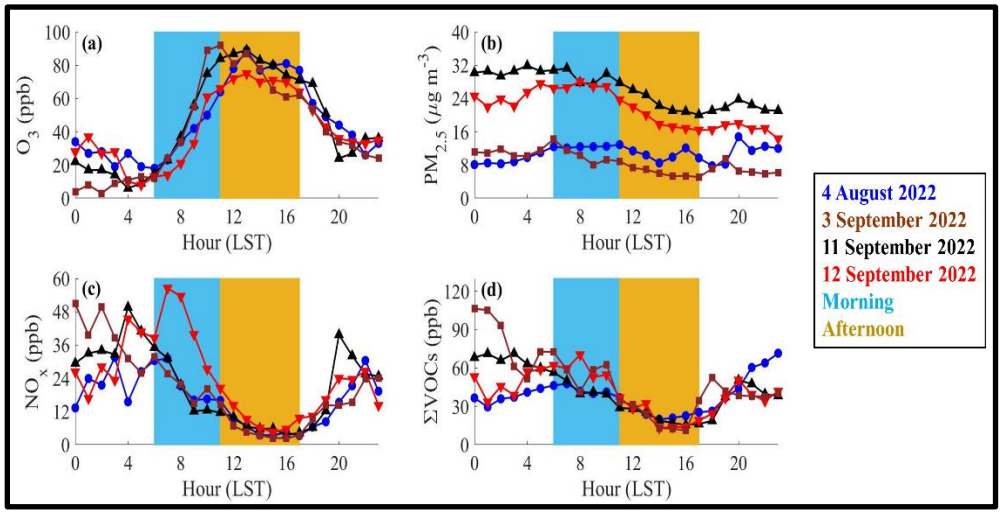

Figure 11. Hour-averaged observations of (a) O_3 (ppb), (b) $PM_{2.5}$ (µg m^{-3}), (c) NO_x (ppb), and (d) ∑VOCs (ppb) on 4 August, 3 September, and 11–12 September.

Table 4. Observed values of maximum daily 8 h average (MDA8) O_3, 24 h average $PM_{2.5}$, daytime (6:00–17:00 LST) median NO_x, daytime median ∑VOCs, and daily maximum temperature (T_{max}) at UTC on the selected case study days.

Date	Classification	MDA8 O_3 (ppb)	24 h $PM_{2.5}$ (μg m^{-3})	NO_x (ppb)	∑VOCs (ppb)	T_{max} (°C)
4 August	Non-smoky weekday	75	10.7	12.7	32.6	34.9
3 September	Weekend day (minimal smoke influence)	76	8.5	10.6	34.2	37.3
11 September	Smoky weekend day	80	26.0	10.8	28.5	30.1
12 September	Smoky weekday	68	21.5	17.3	34.5	32.5

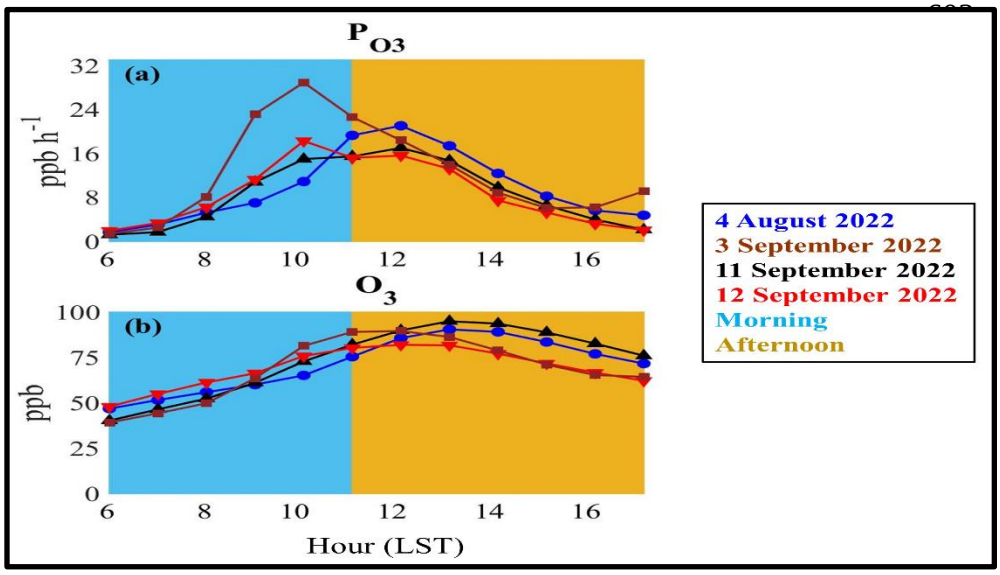

Figure 12. Modeled O_3 production rates (PO_3) and O_3 concentrations for the four case study days.

Daytime values of modeled P_{O3} and O_3 for the base simulations are shown in Figure 12. Across the four days, peak afternoon P_{O3} and O_3 concentrations ranged from approximately 16 to 23 ppb h^{-1} and 82 to 95 ppb, respectively. Several items in Figure 12 stand out. First, P_{O3} and O_3 concentrations increased more rapidly on the morning of 3 September compared to 4 August and 11–12 September. This was likely due in part to higher morning concentrations of reactive VOCs on 3 September (Figure 11), especially formaldehyde, which was very high on the morning of Sept. 3rd. The rapid increase in formaldehyde preceded a rapid increase in O_3, as shown in Figure 13, which suggests that formaldehyde contributed to the high O_3 levels seen on that day and the photochemical modeling supports that conclusion (Figure 12).

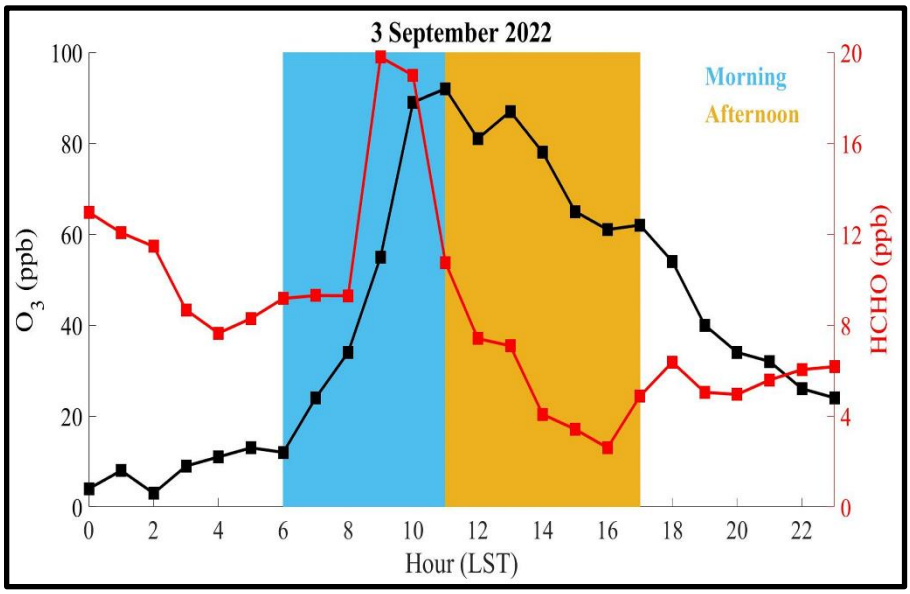

Figure 13. Observed concentrations of O_3 and HCHO on 3 September.

On Sept. 3rd, from 0-10am LST winds at UTC and back-trajectories were from the easterly to southerly directions (ca 90 º -160º) which is the general direction of downtown SLC. While no individual source could be identified to explain the rapid rise in formaldehyde on that day, it seems likely that this increase was due to a source within the urban region. Identifying and controlling this source would likely lead to lower O_3 concentrations in the region. We recommend that future studies in SLC (eg. the 2024 SLC-Summer Ozone Study) could be used to more accurately identify oxygenated VOCs, which are important O_3 precursors.

We also used the photochemical model to examine possible emission reductions of NO_x and VOCs. Figure 14 shows the model calculated O_3 production and O_3 concentrations when anthropogenic VOCs and/or NOx were reduced by various amounts for each of the 4 days.

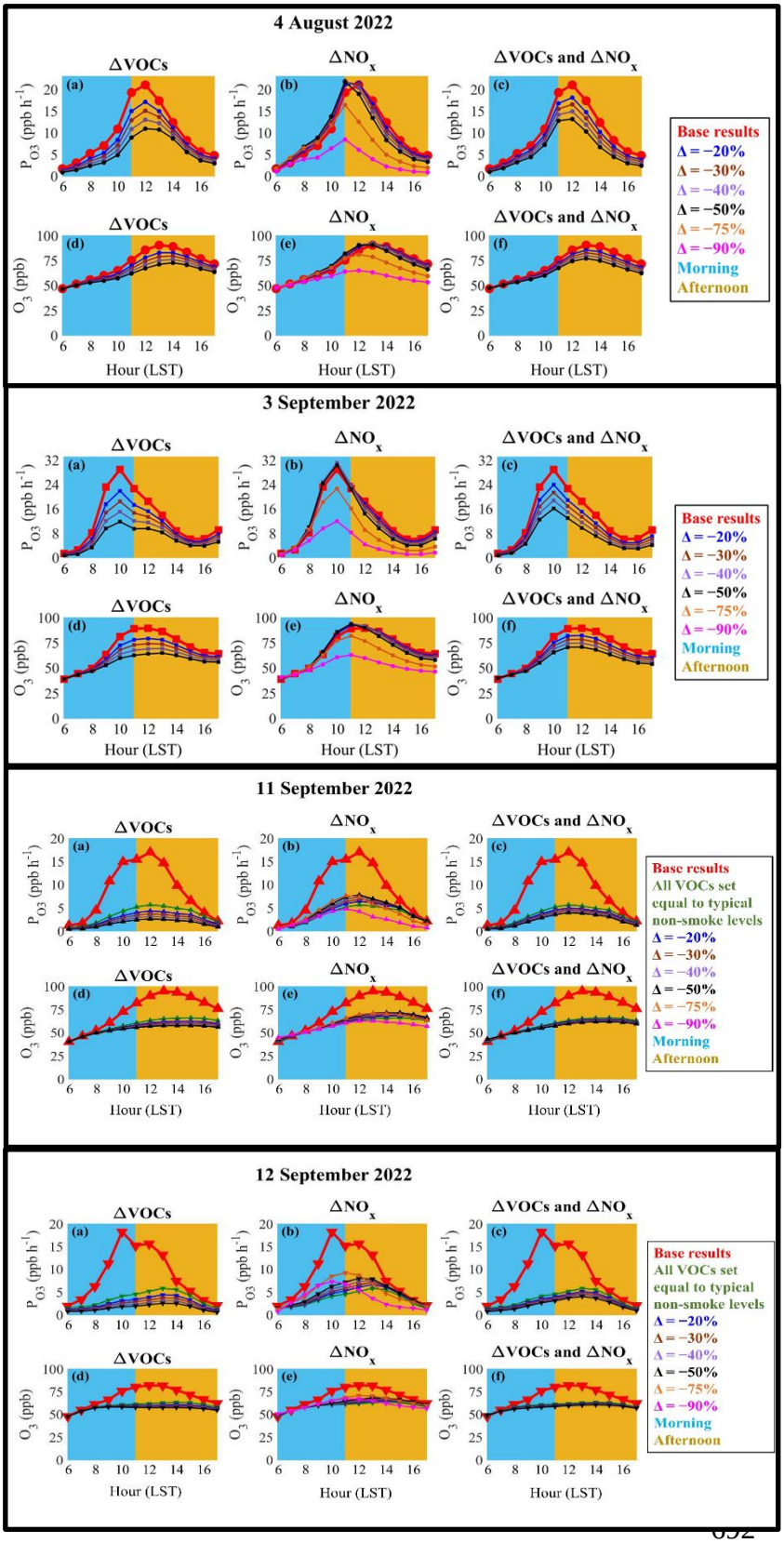

Figure 14. Model-predicted sensitivity to reductions in anthropogenic VOCs and NO_x at UTC. Top row shows P_{O3} and bottom row shows O_3 concentrations for August 4th, September 3rd, 11th and 12th, 2022. For these tests all VOCs were considered anthropogenic except isoprene and monoterpenes. For the two smoky days (September 11th and 12th), smoke VOCs were first reduced by setting these equal to the mean for non-smoky weekends (Sept. 11th) or non-smoky weekdays (Sept. 12th). Then the anthropogenic VOCs or NOx were reduced by the indicated %.

693

The results presented in Figure 14 show that O_3 is most sensitive to VOC reductions and less sensitive to NOx reductions at UTC. Consequently, it is important to determine which VOCs had the greatest impact on O_3 production. To do this, we calculated the observed daytime VOC reactivity for each VOC class ($VOCR_{class}$; s^{-1}) using eq. 4:

$$VOCR_{class} = \sum_i (k_{OH+VOCi} \times [VOC_i]) \quad (4),$$

where $k_{OH+VOCi}$ is the reaction rate coefficient with respect to OH in units of molecule^{-1} cm^3 s^{-1} and [VOC_i] is the concentration of the individual VOCs in molecules cm^{-3}. Figure 15 demonstrates that aldehydes, alkenes, aromatics, and biogenic VOCs (BVOCs) accounted for most of the observed daytime VOC reactivity on the case study days. We note that alkanes were not measured at UTC as part of SAMOZA. However model sensitivity studies using alkane concentrations measured at the Hawthorne site found very little impact on the VOC reactivity or O_3 production (details in Ninneman et al, manuscript in progress). So we conclude these four VOC classes had the most important influence on O_3 formation at UTC. Reducing anthropogenic emissions of aldehydes, alkenes, and aromatics would likely lead to lower O_3 concentrations for the SLC metropolitan area.

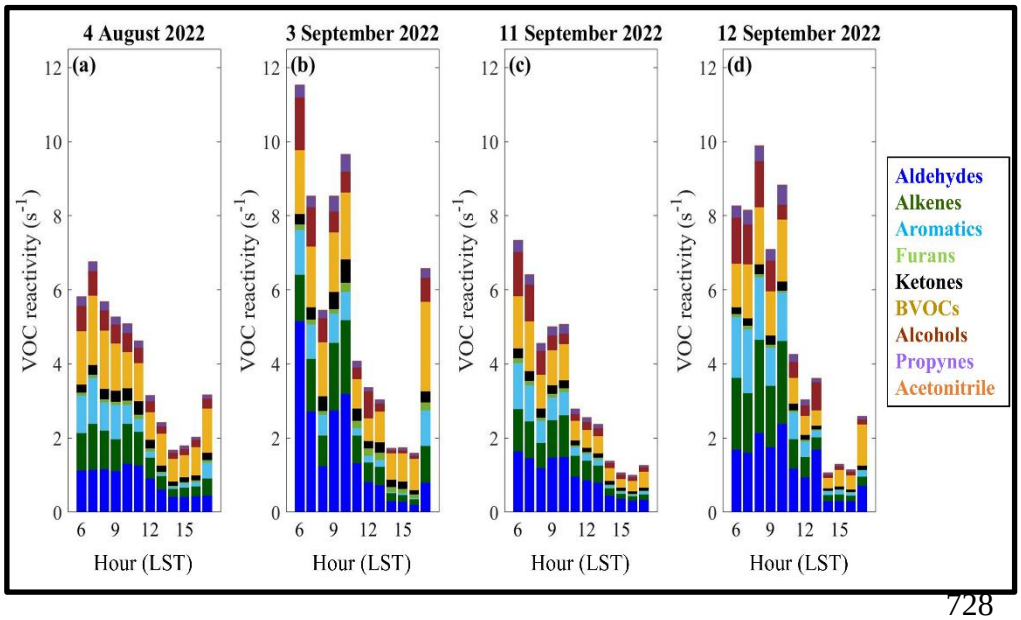

Figure 15. Observed daytime VOC reactivity on (a) 4 August, (b) 3 September, (c) 11 September, and (d) 12 September.

730 Figure 14 shows that removing smoke VOCs has a strong impact on O_3 production. Table 1
731 shows that the sum of measured VOCs increased an average of 56% on smoky days, compared
732 to non-smoke days. However some VOCs increased much more, like formaldehyde, which
733 increased 91% on smoke days, compared to non-smoke days. Figure 16 shows the sensitivity of
734 O_3 production to VOCs on the two smoky days September 11th and 12th. This figure shows that
735 the strong enhancement in O_3 production on these two dates is largely driven by high levels of
736 formaldehyde and other oxygenated VOCs in smoke on those days. The lower O_3 production
737 and O_3 concentrations calculated by the model on Monday September 12th, compared to the
738 Sunday 11th, were likely associated with NOx suppression, due to the high concentrations of
739 NOx seen on that day (as seen in Figures 6 and 7).
740
741

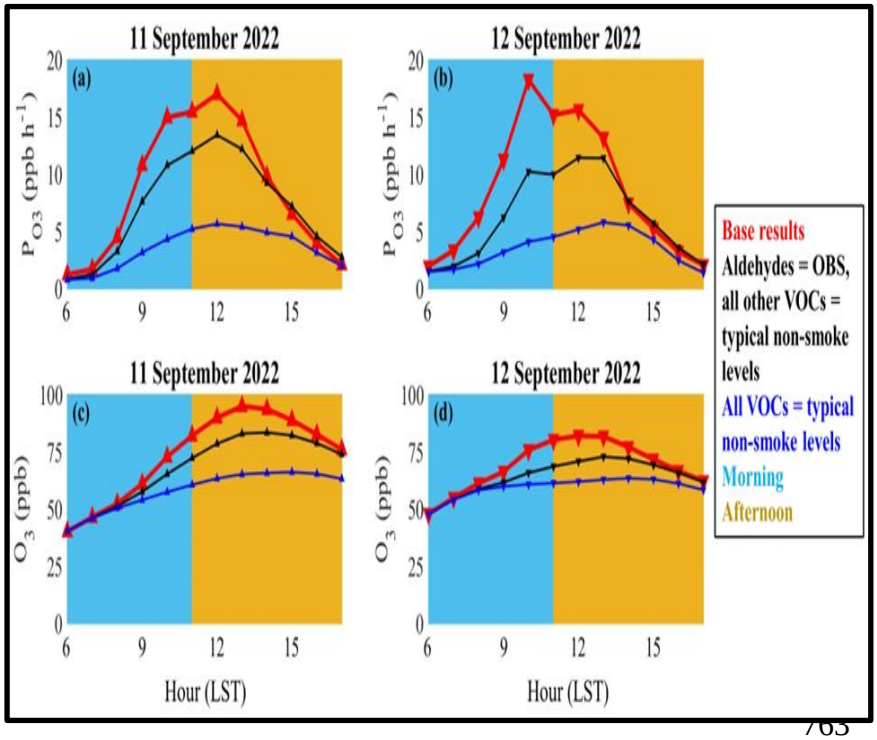

Figure 16. Impact of VOCs on model calculated PO3 (top row; panels (a) and (b)) and O3 (bottom row; panels (c) and (d)) on 11 September (first column) and 12 September (second column), two smoke influenced days. Red line shows base results where all VOCs and NOx were constrained by observed values. Black line shows model results when all VOCs except aldehydes were reduced to the values seen on non-smoky weekend (Sept 11th) or non-smoky weekdays (Sept 12th). Blue line shows model results when all VOCs, including aldehydes, were reduced to the values seen on non-smoky weekend (Sept 11th) or non-smoky weekday (Sept 12th).

763
764
765 Because UTC is one of the highest-NO_x sites in the SLC metropolitan area, we want to consider
766 how these results will apply to other parts of the SLC region. During August–September 2022,
767 the observed mean 24 h average NO_2 concentration at UTC was 13.4 ppb, which was 56%
768 greater than the regional mean of 8.6 ppb measured by UDAQ at 9 sites in the SLC Core Based
769 Statistical Area (CBSA) . On the two case study days with little to no smoke influence – 4

August and 3 September – the NO_x sensitivity tests indicated that NO_x reductions of 75% or greater are needed to noticeably reduce O_3 concentrations at UTC (Figure 14). Based on the observed mean 24 h average NO_2 concentrations at UTC versus the entire region from August–September 2022, a 75% reduction in NO_x at UTC corresponds to an approximately 60% reduction in NO_x regionwide. Further details and sensitivity tests using the photochemical box model will be presented in a scientific publication that is currently in-progress (Ninneman et al: Investigation of Ozone Formation Chemistry During the Salt Lake Regional Smoke, Ozone, and Aerosol Study (SAMOZA)).

a. Generalized Additive Model

GAMs are a type of machine learning/statistical model that uses observations to train a dataset to predict a specific parameter. GAMS are particularly useful for air quality applications as they can incorporate linear, non-linear and categorical variables to predict the O_3 MDA8. Typical predictors include meteorological variables, such as the daily maximum temperature or geopotential height, day of week, back-trajectory distance and direction, surface chemical measurements (e.g., NO_x and VOCs) and satellite observations. Our group has used GAMs to quantify the additional O_3 associated with smoke in numerous urban areas, including SLC (Gong et al., 2017; Jaffe, 2021). In addition, we have applied this approach in several successful exceptional event demonstrations to quantify the influence of smoke on the O_3 MDA8 (LDEQ, 2018; TCEQ, 2017). For SAMOZA, we improved the GAM results from our previous work and extended the analysis through September 2022.

We used data from four sites in SLC. For two sites, Hawthorne, and Bountful Viewmont, we used data for May-September 2006-2022. For Erda and Herriman data are only available for 2015-2022. For each site, the data were split into smoke and no-smoke days, using the same criteria as given above (overhead HMS smoke plus $PM_{2.5}$ > mean+1 SD of annual May-September mean for non-HMS days). For the GAM model evaluation, the no-smoke data were further split into training (90%) and test data (10%), where the test data are rotated through the whole dataset and the model evaluation is repeated ten times (10-fold cross validation).

Since the distribution of MDA8 O_3 was close to a normal distribution, Gaussian distributions and the identity link function were used in this study. Penalized cubic regression splines with ten basis functions (i.e., k = 10) was used. For the analysis, we used the "gam"

function in the "R" software mgcv package with univariate smooths and/or bivariate smooths (i.e., in interactions). Note that the number of "k" for "YEAR" smooth term was set to 6 for the HW and BT sites, and 3 for the HR and ER sites. This approach, based on suggestions in previous study (Walker et al., 2022), was employed to avoid overfitting with respect to the temporal trends in the data. When increasing the k value, overfitting occurs at some sites (particularly, HR and ER sites), resulting in high R^2, but bias occurs for certain parts of the data. We tested GAM models through a variety of combinations and then determined the final version of the GAM model by considering main effects and interactive influencing factors as shown in the Lee et al (to be submitted). In addition, we conducted 10-fold cross validation on the GAM model to evaluate its performance. This involved partitioning the data into training data (90% of the total) and test data (10% of total), which is repeated 10 times. Table 5 shows a list of the predictors used and Table 6 shows the form for the final GAM model chosen.

Table 5. List of predictors used in the GAM modeling for SAMOZA

Source*	NO.	Parameter	Unit	Description
1	1	DOW	-	Day of week (factor, from Mon to Sun)
	2	DOY	-	Day of year (from 1 to 365/366)
	3	YEAR	-	Year (from 2006 to 2022)
2	4	Tmax	ºF	Daily maximum temperature at SLC airport (40.77º N, 111.96º W)
	5	RH	%	Daily average relative humidity at SLC airport (40.77º N, 111.96º W)
	6	DewP	ºF	Daily average dew point at SLC airport (40.77º N, 111.96º W)
3	7	TPW	kg m^{-2}	Daily average total precipitable water in the entire atmospheric column
	8	T700	K	Daily average air temperature at 700 hPa
	9	MW10m	m s^{-1}	Daily average meridional wind at 10 m above the ground
	10	ZW10m	m s^{-1}	Daily average zonal wind at 10 m above the ground
	11	MW700	m s^{-1}	Daily average meridional wind at 700 hPa
	12	ZW700	m s^{-1}	Daily average zonal wind at 700 hPa

4	13	TM1000	ºF	Morning temperature in lowest 1000 m
5	14	NO2VCD	molec. cm^{-2}	OMI NO_2 Vertical Column Density (VCD) in the range of 40.25–41.25º N and 111.50–112.25º W
	15	CLFR	-	OMI Cloud fraction in the range of 40.25–41.25º N and 111.50–112.25º W
6	16	TrajDist	km	Endpoint distance (point to point) after 12 hours of transport for a back trajectory initialized at 1pm local time
	17	TrajDir	deg	Endpoint direction (point to point) after 12 hours of transport for a back trajectory initialized at 1pm local time

Table 6. The final version of the GAM model in this study

$$MDA8\ O_3 = \beta_0 + DOW + s(DewP, RH) + te(TrajDist, TrajDir) + \sum_{j=1}^{n} s(x_j) + \sum_{k=1}^{m} ti(X_k) + e \quad (6)$$

x_j: YEAR, DOY, Tmax, TPW, T700, MW10m, ZW10m, MW700, ZW700, TM1000, NO2VCD, and CLFR

X_k: (YEAR, Tmax), (DOY, Tmax), (DOY, RH), (DOY, DewP), (Tmax, MW10m), and (Tmax, MW700)

s(): The function of modeling the main effects only, or the main effects and interactions between covariates (the same basis function is used for each covariate)

te(): The function of modeling the main effects and interactions between covariates (different basis function is used for each covariate)

ti(): The function of modeling interactions between covariates without including the main effects

Figure 17 shows the results from the GAMs for the four sites. R^2 for the four sites range 0.59-0.66. Figure 18 shows the residuals (observed – GAM predicted) for each site as a function of the prediction value and smoke/no smoke condition and Tables 7 and 8 show statistics on the residuals for the training, test and smoke datasets. As we have seen previously, the GAM results are unbiased for the non-smoke days, but have a significant positive bias on smoke days, associated with the greater than expected amount of O_3 for the specific meteorological conditions.

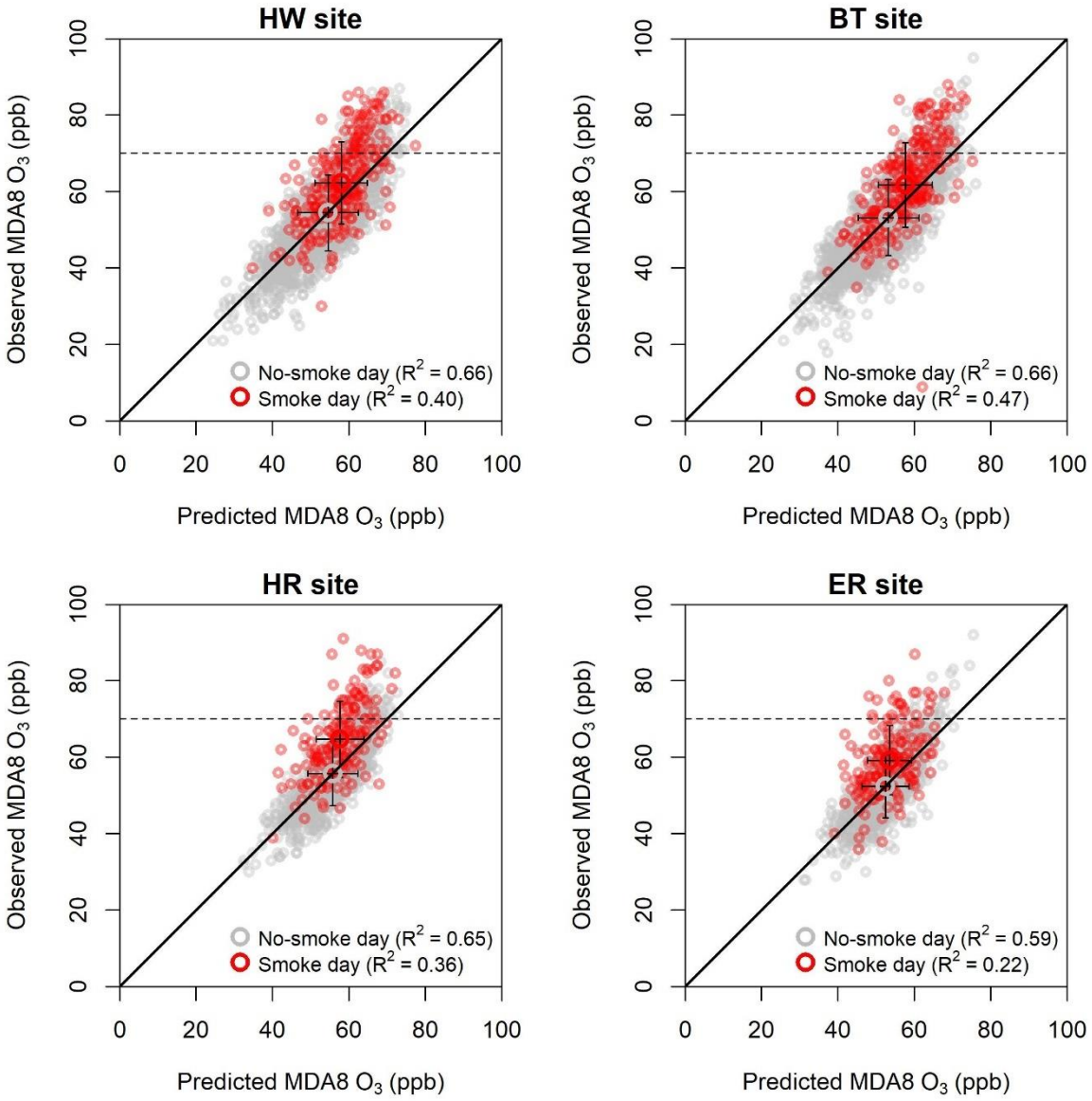

Figure 17. Observed MDA8 O_3 vs. Predicted MDA8 O_3 using GAM models. The solid line represents 1:1 line, and the dashed line represents the NAAQS standard (i.e., 70 ppb). The small open circle represents the daily points corresponding to observed and predicted MDA8 O_3, and the large open circle represents the overall mean of observed and predicted MDA8 O_3 for both no-smoke and smoke days, while the error bars represent the standard deviation. (HW=Hawthorne, BT=Bountiful, HR=Herriman and ER=Erda).

839

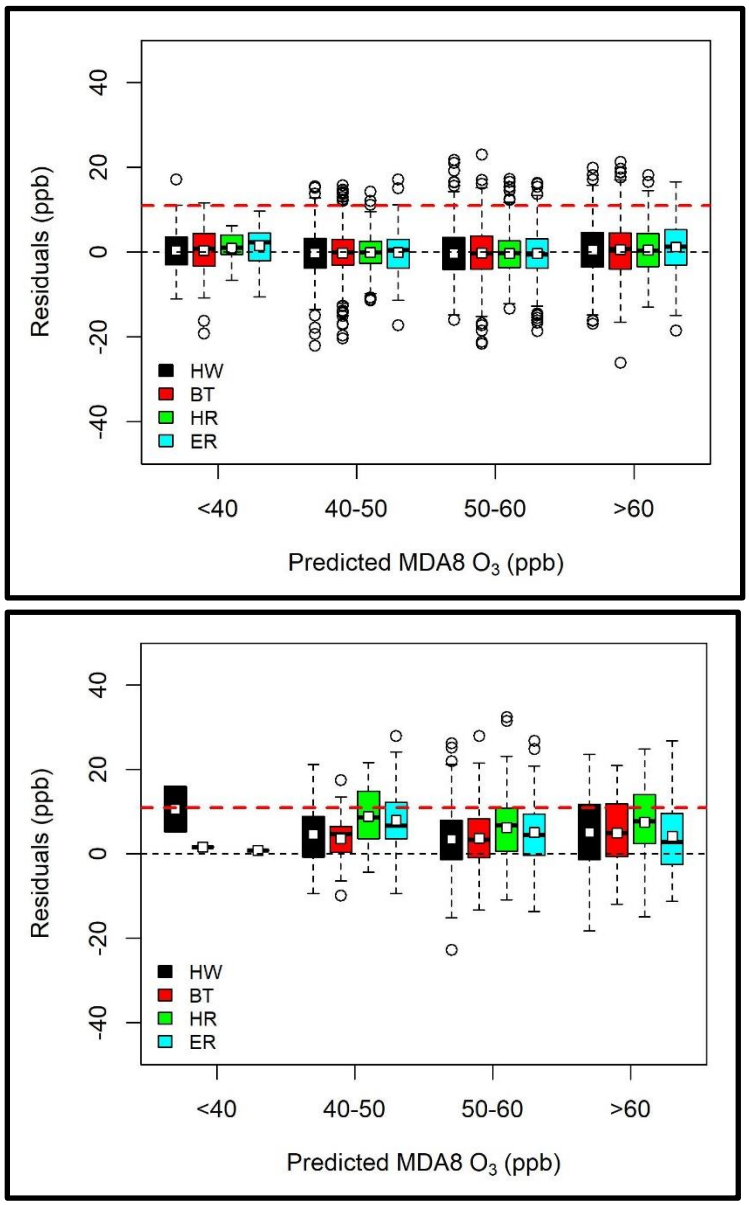

Figure 18. Residuals vs. Predicted MDA8 O_3 (i.e., the model fit) for no-smoke days (top) and smoke days (bottom) at all sites. Boxes and whiskers represent the 25th–75th percentiles and 1.5 times interquartile range (1.5IQR), respectively; squares indicate means and horizontal lines within boxes indicate medians; the dashed red line indicates the average 97.5th percentile of residuals on no-smoke days for all sites (10.9 ppb).

Table 7. Summary of GAM results using 10-fold cross validation.

Dataset	Site	R^2	Residuals (ppb)
Training data	HW	0.66	0.0 ± 5.8
	BT	0.66	0.0 ± 5.8
	HR	0.65	0.0 ± 5.0
	ER	0.60	0.0 ± 5.3
Test data	HW	0.61	–0.01 ± 6.2
	BT	0.60	–0.01 ± 6.2
	HR	0.57	0.02 ± 5.5
	ER	0.49	0.00 ± 5.9

Table 8. GAM residuals statistics for smoke and non-smoke days.

Site	Smoke day residuals (ppb)	Smoke day positive residuals (ppb)	95th percentile of residuals (no smoke, ppb)	97.5th percentile of residuals (no smoke, ppb)
HW	4.4 ± 8.3	8.2 ± 5.9	9.5	11.5
BT	4.2 ± 8.1	7.6 ± 5.5	9.4	11.5
HR	7.1 ± 8.0	9.5 ± 6.5	8.1	10.3
ER	5.8 ± 8.2	8.8 ± 6.5	8.3	10.5
Avg.	5.1 ± 8.2	8.5 ± 6.1	8.8 ± 0.7	10.9 ± 0.7

Table 9. Percentage of days exceeding the EPA (2015) threshold (97.5th percentile of residuals (10.9 ppb) to support exceptional event cases for smoke and non-smoke days and contribution to the MDA8 using the EPA 2015 methodology.

Site	Smoke days			No-smoke days		
	N (%)	MDA8 O_3 (ppb)	MDA8 O_3 contribution (ppb)	N (%)	MDA8 O_3 (ppb)	MDA8 O_3 contribution (ppb)
HW	22	74.3 ± 7.9	4.6 ± 3.7	3	71.2 ± 9.1	2.7 ± 2.5
BT	19	74.9 ± 7.5	4.2 ± 3.5	3	70.9 ± 9.2	3.0 ± 2.7
HR	31	74.5 ± 7.8	5.4 ± 4.5	2	71.0 ± 7.9	2.5 ± 2.2
ER	22	69.9 ± 7.0	6.5 ± 4.6	2	70.6 ± 8.4	2.9 ± 2.0
Avg.	-	73.6 ± 7.8	5.1 ± 4.2	-	71.0 ± 8.8	2.8 ± 2.4

[1]EPA, U. S., "Guidance on the Preparation of Exceptional Events Demonstrations for Wildfire Events that May Influence Ozone Concentrations", 2015. Retrieved from: https://www.epa.gov/sites/production/files/2015-11/documents/o3_draft_wildfire_guidance.pdf.

The EPA suggests that states use a 97.5th percentile criteria of residuals to determine smoke impacts on the MDA8 (U.S. EPA 2015). Table 9 shows that of the non-smoke days, only 2-3% of these days meet this criteria, which is expected from the statistical distribution. In contrast, we find that 19-31% of the smoke days, exceed this criteria and thus the GAM results could be used to support exceptional event documentation for these days. Table 9 also shows that the average O_3 contribution for these days is 5.1 ppb, calculated using the guidance provided in U.S. EPA (2015). Further details and sensitivity tests using the machine learning/Generalized Additive Modeling will be presented in a scientific publication that is currently in-progress (Lee et al: Evaluating the impact of wildfire smoke on ozone concentrations using a Generalized Additive Model in Salt Lake City, Utah, USA, 2006–2022).

Comparisons of PTRMS and DNPH data

We compared two methods to identify carbonyls: proton transfer reaction mass spectrometry (PTR-MS) and collection on 2,4-dinitrophenylhydrazine (DNPH)-coated cartridges followed by analysis by high-performance liquid chromatography (HPLC). PTR-MS and DNPH-HPLC methods quantified four compounds in common: formaldehyde, acetaldehyde, acetone, and 2-butanone. Correlation analysis of the two methods indicates a high positive correlation in acetone, formaldehyde, acetaldehyde, and 2-butanone (r^2 = 0.83, 0.72, 0.69, and 0.65, respectively). However, the slopes of the correlations were 1.03, 0.34, 0.41, and 0.32, respectively, indicating that the DNPH-HPLC method resulted in similar amounts of acetone—but less formaldehyde, acetaldehyde, and 2-butanone—than the PTR-MS method (Figures 19-22).

Non-target compounds can interfere with target compounds with the same mass in the PTR-MS method, resulting in a high bias (this is a known problem for aldehydes; Vlasenko et al. (2010)). For the DNPH-HPLC method, interference from atmospheric constituents can generate low and high biases (Ho et al., 2013). We used potassium iodide cartridges to eliminate interference from ozone, but other interferents are possible.

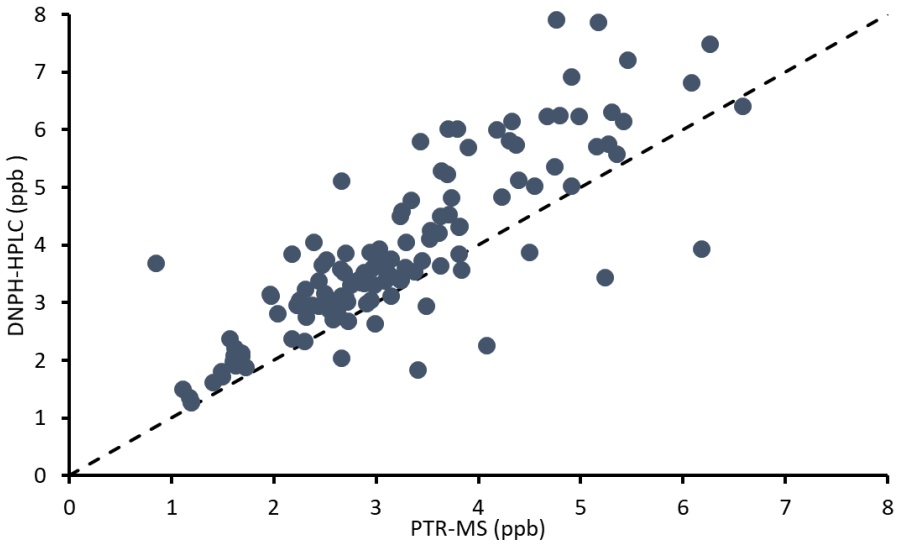

Figure 19. Comparison of acetone measurements from PTR-MS and DNPH-HPLC methods. The 1:1 line is also shown.

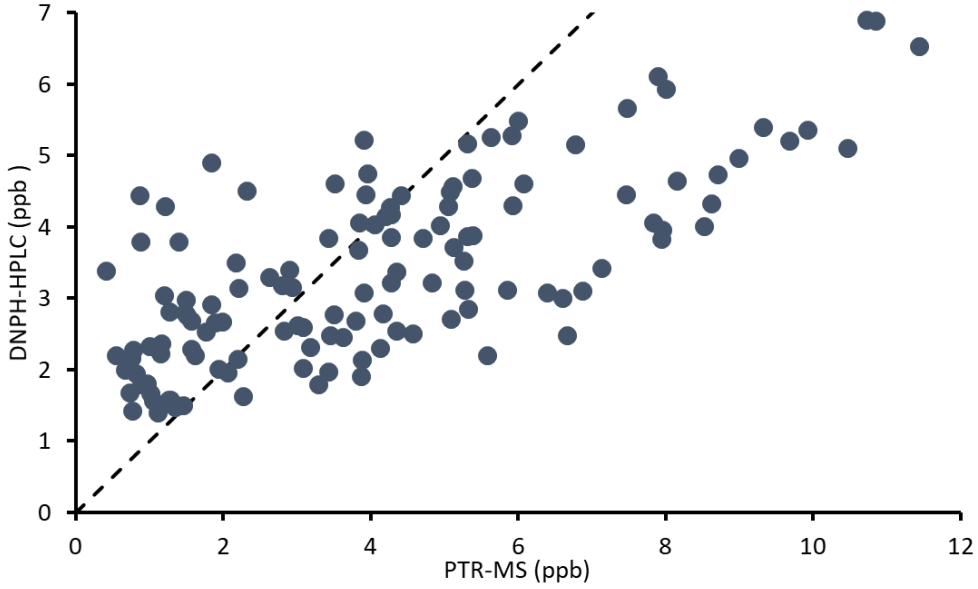

Figure 20. Comparison of formaldehyde measurements from PTR-MS and DNPH-HPLC methods. The 1:1 line is also shown.

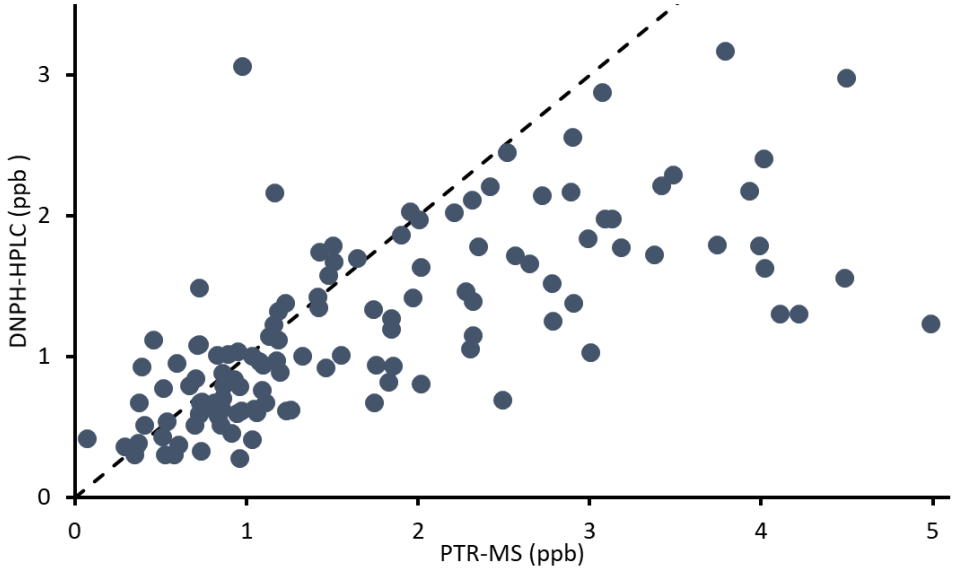

Figure 21. Comparison of acetaldehyde measurements from PTR-MS and DNPH-HPLC methods. The 1:1 line is also shown.

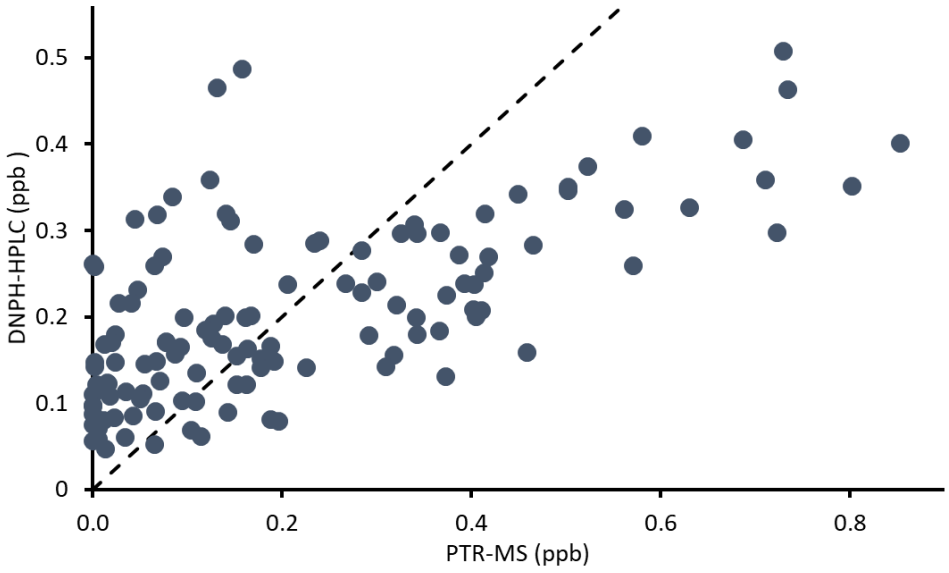

Figure 22. Comparison of 2-butanone measurements from PTR-MS and DNPH-HPLC methods. The 1:1 line is also shown.

PTR-MS measurements of carbonyls were used in the modeling work described above. When DNPH measurement-derived values for the four carbonyls shown in Figures 16-19 were used in the model, 1-hr maximum modeled ozone decreased by 2, 14, and 9% for August 4, September 11, and September 12, respectively. PTR-MS and DNPH measurements were more different on smoke days than non-smoke days (Table 1), so the change in carbonyls was greater on

September 11 and 12 than August 4. The greater difference between the two methods on smoke days could be caused by interference in one or both measurement systems. The cause of these differences is still under investigation by the SAMOZA team.

When all modeled carbonyls, not just the ones measured in common by PTR-MS and DNPH, were set to match DNPH-derived values, 1-hr maximum modeled ozone changed by less than 1% relative to the change to just the four carbonyls in Figures 16-19, likely because mixing ratios of those carbonyls were very low (0.5 ppb or less).

e. Positive Matrix Factorization

Positive matrix factorization (PMF) is an analysis technique that often affords clues about source apportionment in an air shed. We performed a PMF analysis on the concentration data of the ten compounds listed in Table 10. All available hourly average data for the dates 2022-08-01 to 2022-09-30 were included in the analysis.

The analysis is based on the following mathematical model of the data. Let C_{tc} represent the concentration of compound c at time t. We assume there are a number of sources or factors, each one possessing its own temporally-uniform concentration signature. Let X_{sc} represent the mole fraction of compound c in source s. As a mole fraction, X_{sc} is unitless and its sum over compounds is 1: $\sum_c X_{sc} = 1$. We assume that T_{ts} concentration units of source s are present at time t, so that $T_{ts}X_{sc}$ represents the concentration of compound c derived from source s at time t. Summing over all sources yields the modeled concentration of compound c at time t:

$$C'_{tc} = \sum_s T_{ts}X_{sc} \qquad (7)$$

The prime is used to distinguish modeled and measured concentrations. In our work, T_{ts}, C_{tc}, and C'_{tc} are in ppb units. Note that this equation represents a matrix product. Therefore, the procedure consists of determining two initially unknown matrices T_{ts} and X_{sc} that optimize the fit between C_{tc} and C'_{tc}. [Paatero & Tapper (1994)] Because negative values of T_{ts} and X_{sc} are physically excluded, the optimization must be carried out subject to the constraints $T_{ts} \geq 0$ and $X_{sc} \geq 0$. Hence the expression "positive matrix factorization."

We used the EPA Positive Matrix Factorization 5.0 tool [Norris et al. 2023] to perform the optimization. The number of sources is a variable in the calculation; we used the default value of 6. We performed about 20 independent runs with unique random seeds to verify that the analysis converged consistently to the same solution.

Table 10. Compounds included in the PMF analysis.

acetonitrile	isoprene
acetone	acetaldehyde
benzene	methanol
butenes	methyl vinyl ketone + methacrolein (MVK + MACR)
formaldehyde	toluene

Scatter plots for all pairs of compounds were examined. Some of these display interesting structure related to diurnal trends in the concentrations. Figure 23 shows such a plot for the concentrations of toluene and acetone. The data are separated into eight sets by month, August or September, and by time of day, predawn, morning, afternoon, or evening. Least-squares lines for each set are also shown, colored to indicate the time of day, while solid and dashed lines correspond to the months of August and September, respectively. Afternoon data pile up near the base of the plot, and the least-squares slopes of the predawn data are about nine times larger than the slopes of the afternoon data. As explained fully below, the most logical explanation is photochemical formation of some compounds under the afternoon sun.

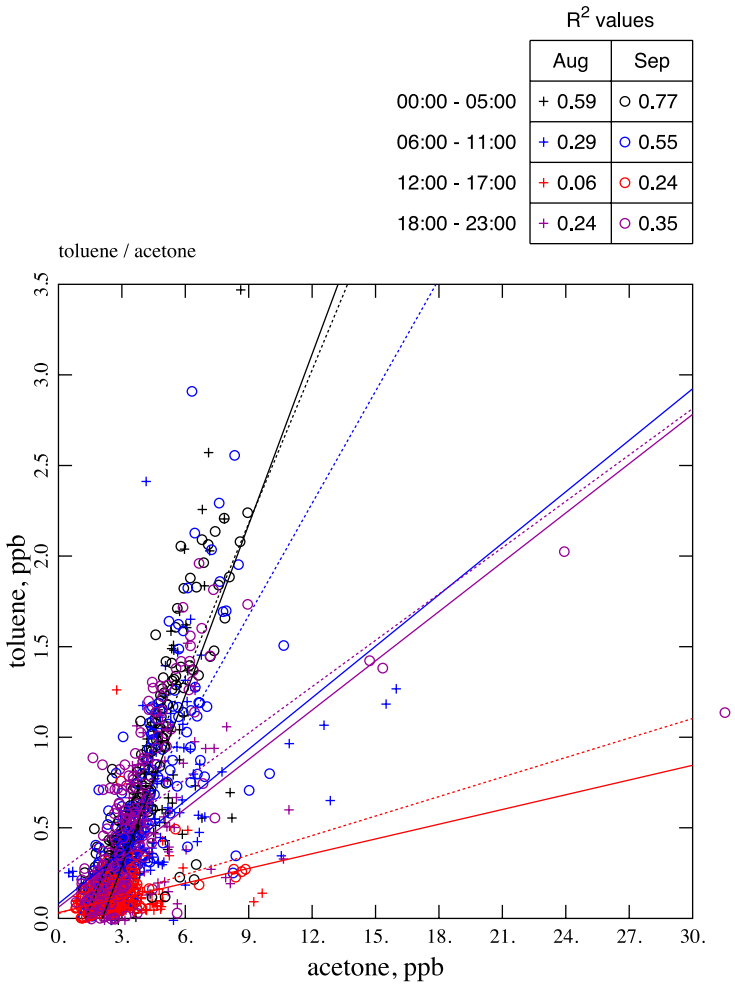

965

966 **Figure 23. Scatter plot of toluene vs. acetone concentrations. Eight different datasets,**
967 **corresponding to the two months of August and September, and to predawn, morning, afternoon**
968 **and evening time periods, are shown. Least-squares lines corresponding to each dataset are also**
969 **shown. Solid and dashed lines correspond, respectively, to August and September data.**

970

971 The six sources obtained from the PMF calculation are summarized as pie charts in Figure 24.
972 Sources A, B, and E are dominated by formaldehyde, methanol, and acetone, respectively.
973 Acetaldehyde is a majority component of source C. Figure 25 confirms the quality of fit
974 between between C_{tc} and C'_{tc} for two selected days. Comparable fits are seen for all 61 days.

975

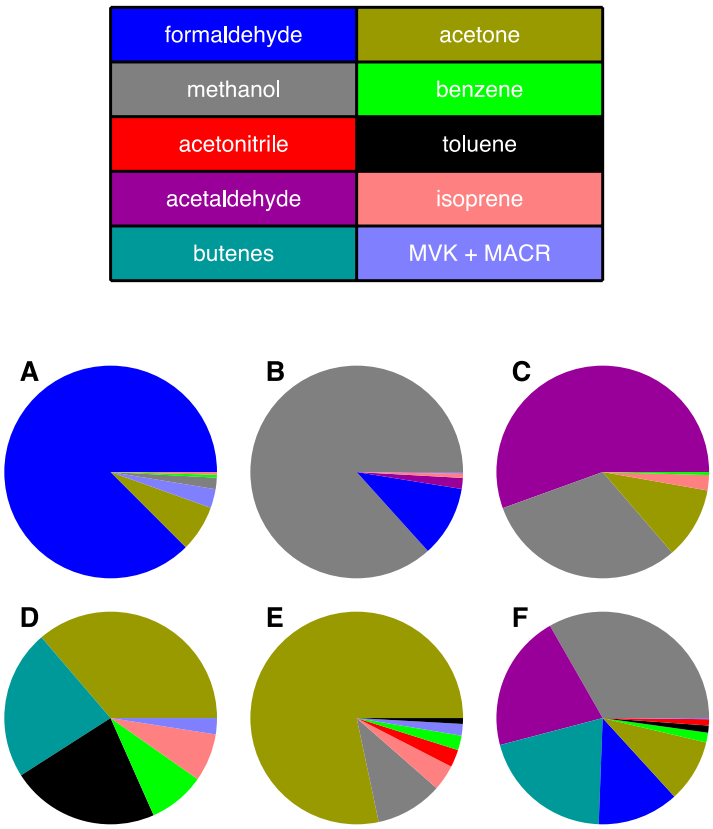

976

977 **Figure 24. The PMF analysis identified six sources, labeled A through F, with the indicated**
978 **speciation profiles.**
979

980

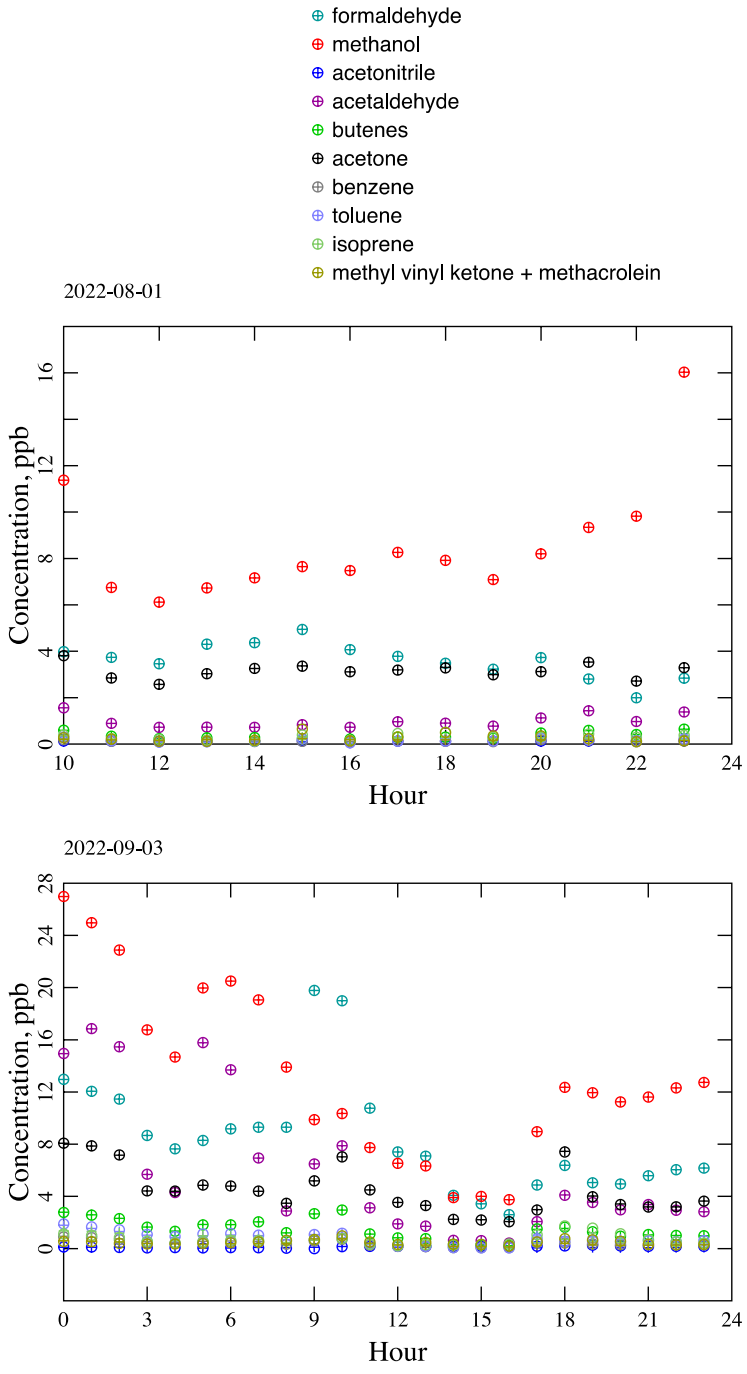

981

982 **Figure 25. Comparison between measured (open circles) and modeled (crosses) concentrations for**
983 **two different days. The measured and modeled concentrations agree to within the resolution of this**
984 **plot.**

985

986

Figure 26 displays the average concentration contributed by each of the six sources at each hour of the day, normalized relative to each maximum. All six sources show a dip in the afternoon, not surprising because we expect dilution resulting from mixing of the atmosphere. However, sources C, D, and F dip to values around 10% or 20% of their maxima, while B, A, and E dip to about 30%, 50%, and 80%, respectively, of theirs. If dilution caused by meteorology were the sole explanation for the dips, we would expect all six dips to be of comparable size. Rather, it appears that compounds dominated by sources A and E, and probably B, are created in processes that are stronger in the afternoon and that partially compensate for the meteorological dilution. Presumably, some compounds are formed photochemically under the afternoon sun.

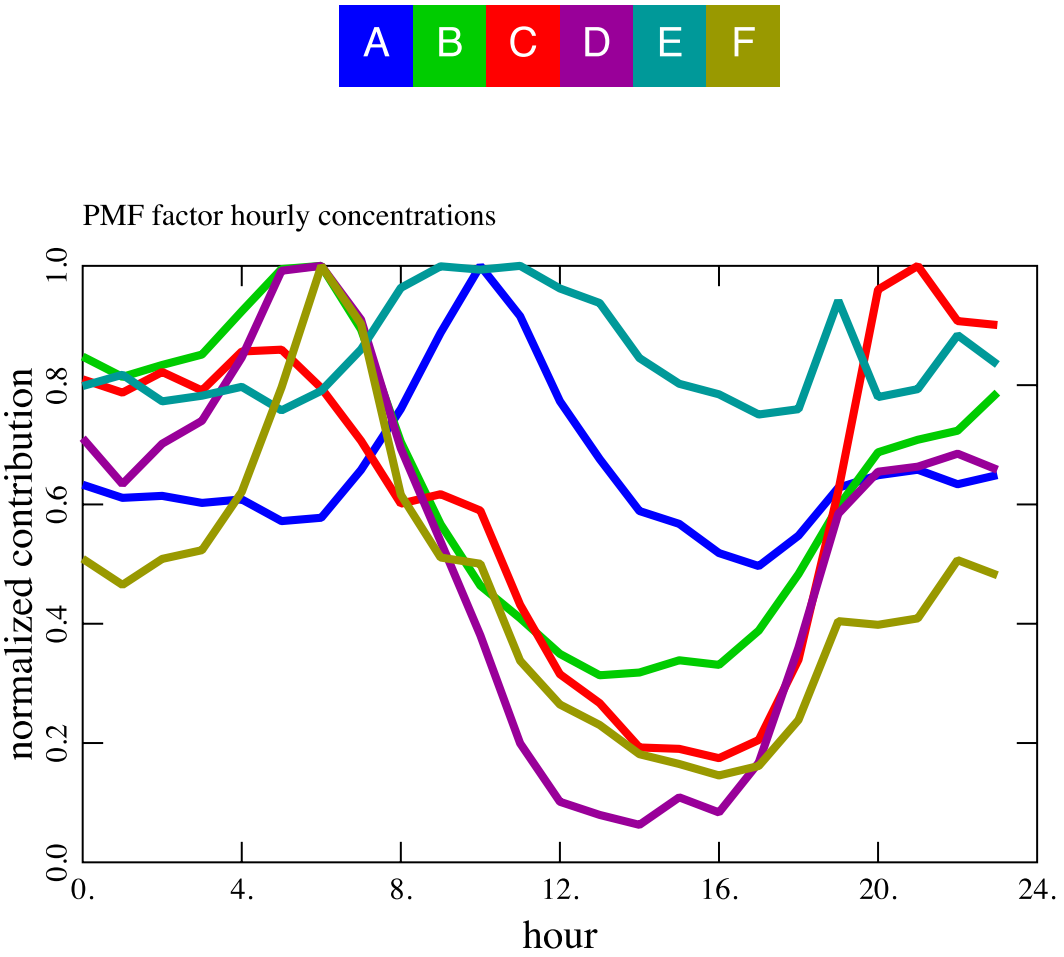

Figure 26. Average concentration of each of the six sources at each hour of the day, normalized relative to the maximum.

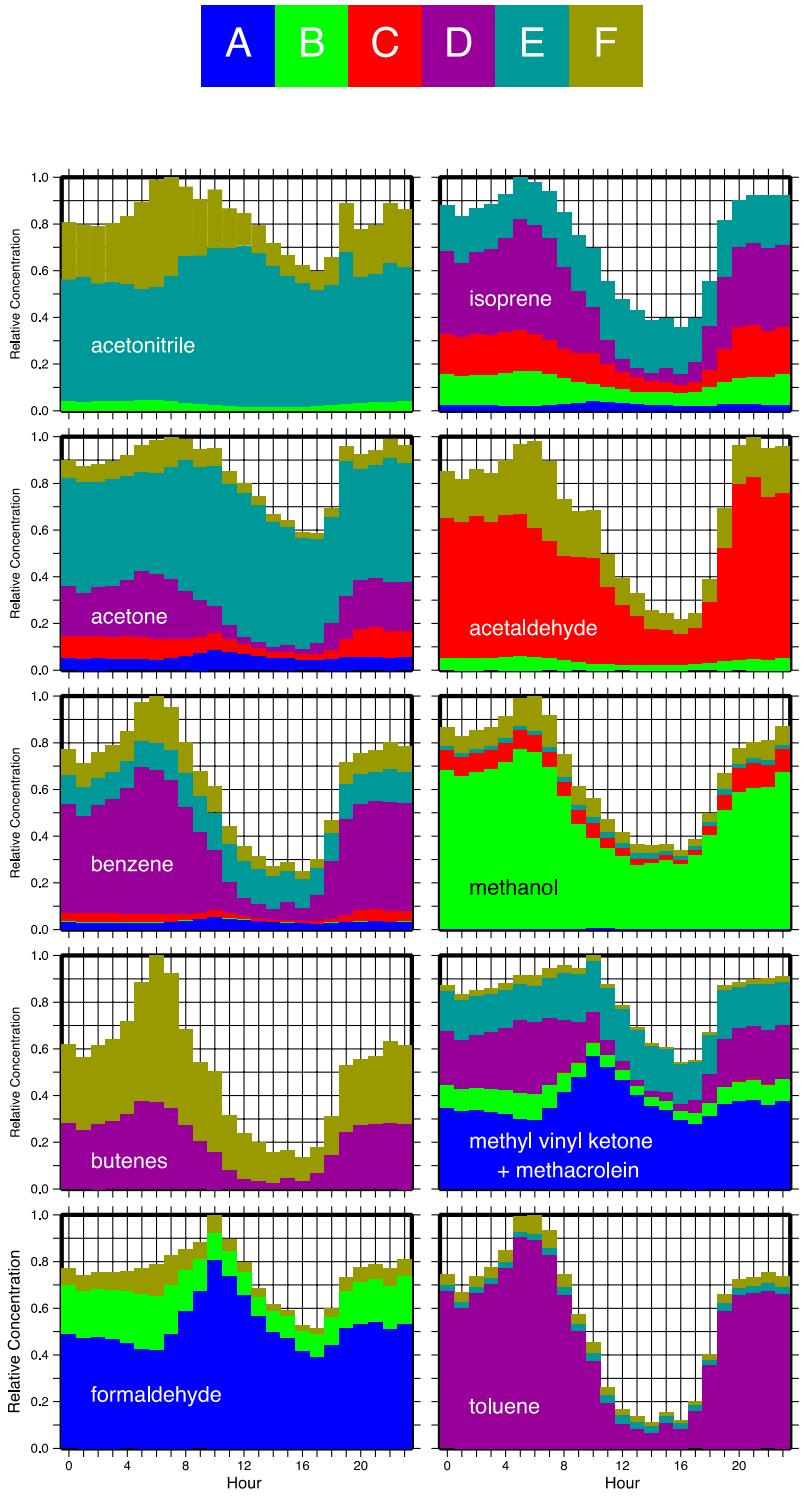

Figure 27. Average concentrations of ten compounds at each hour of the day, normalized relative to their maximum.

Figure 27 displays diurnal variations in the concentrations of the ten compounds. Toluene and benzene are dominated by source D, and the butenes by sources D and F, indicating little or no secondary formation. Acetone and formaldehyde are dominated, respectively, by source E and A, implying secondary formation. Indeed, there is independent evidence for secondary formation of formaldehyde and acetone. That of formaldehyde is documented in the box model results given by Ninneman et al (in preparation), while Hu et al. [2013] estimate that about 50% of the North American acetone budget is contributed by secondary formation. The MVK + MACR signal has important contributions from sources A and E, but since these compounds are known to form biogenically, we may in fact be seeing a biogenic production that intensifies in the afternoon. Interestingly, one might expect to see secondary acetaldehyde formation in parallel with that of formaldehyde, but we see no strong evidence for it.

Discussion and implications

The SAMOZA team measured a suite of VOCs, CO and O_3 (using a novel "scrubber-less" method) at the UTC site in SLC during August-September 2022. Along with the standard UDAQ observations, the SAMOZA data have been used to support a variety of analyses. The main conclusions from SAMOZA are as follows:

1. We found no evidence for bias in smoke from the standard O_3 measurements made by UDAQ using a Teledyne T400 instrument at $PM_{2.5}$ concentrations up to 60 μg m^{-3};
2. Formaldehyde (CH_2O) and other aldehydes are key O_3 precursors. We measured formaldehyde by two different methods and these showed generally good correlation, but the PTR-MS measurements are approximately 50% greater than the DNPH measurements on smoky days. The cause for this difference is not yet known.
3. There appear to be primary sources of formaldehyde in the SLC urban region. Identifying and controlling these sources could lead to significant reductions in regional O_3;
4. On days with smoke, we found that $PM_{2.5}$, CO, O_3 and nearly all VOCs were significantly enhanced. While all VOCs contribute to the increase O_3 production on smoke days, aldehydes are the strongest contributor.

5. Photochemical modeling of O_3 production rates at the Utah Tech Center demonstrates a strong sensitivity to VOC concentrations and less sensitivity to NO_x. For non-smoke days, reductions in VOCs of ~30% would result in significantly reduced O_3 production, potentially meeting the O_3 standard. Reductions in NO_x of ~60% are needed to get a significant reduction in O_3 production for non-smoke days. VOCs with the greatest contribution to O_3 production are oxygenated VOCs, along with alkenes.

6. Generalized Additive Modeling (GAM) gave similar MDA8 O_3 enhancements on smoky days as the photochemical modeling. Analysis of the GAM results show that 19-31% of the smoke days have model residuals that exceed the EPA (2015) criteria for statistical analysis of O_3 data, and thus this method could be used as support for exceptional event cases for those days.

Complete SAMOZA publication list (all papers are currently in progress and expected to be submitted by the end of 2023:

We note that several of the analyses results presented here are still in progress and thus should be considered preliminary. Further details and refined analyses will be presented in several scientific publications:

Cope E., et al., Sources of VOCs in SLC.

Lee H., et al: Evaluating the impact of wildfire smoke on ozone concentrations using a Generalized Additive Model in Salt Lake City, Utah, USA, 2006–2022). In-review for the J.Air Waste Management Association.

Jaffe D.A., et al: An Overview of the Salt Lake Smoke, Ozone and Aerosol Experiment (SAMOZA). In-review for the J.Air Waste Management Association.

Ninneman M., et al: Investigation of Ozone Formation Chemistry During the Salt Lake Regional Smoke, Ozone, and Aerosol Study (SAMOZA)

Data availability statement

Final SAMOZA data has been archived at the University of Washington ResearchWorks archive: http://hdl.handle.net/1773/50049

Results and R codes for the GAM analysis have been supplied to the Utah Division of Air Quality

Acknowledgements

The SAMOZA team consisted of faculty, students and post-doctoral fellows from the University of Washington, University of Montana and Utah State University. In addition to the Principal Investigators (Jaffe, Hu and Lyman) the team included:

Matt Ninneman, Linh Nguyen and Haebum Lee (University of Washington)

Colleen Jones, Trevor O'Neil and Marc Mansfield (Utah State University)

Damien Ketcherside, Lixu Jin and Emily Cope (University of Montana)

We thank the entire team for their contributions to this project!

SAMOZA could not have happened without funding from the Utah Division of Air Quality through a Science for Solutions grant to the three universities. We further acknowledge support from several industry partners including:

Rio Tinto Kennecott Utah Copper, LLC.

Tesoro Refining and Marketing Co.

Holly Frontier Woods Cross Refining LLC.

Big West Oil LLC.

Chevron USA Inc.

The Utah Division of Air Quality reviewed the draft report and made suggestions for the final version. The industry partners had no input on the experimental design or interpretation of the data and results presented in this report.

References cited

Alvarado, M.J.; Lonsdale, C.R.; Yokelson, R.J.; Akagi, S.K.; Coe, H.; Craven, J.S.; Fischer, E.V.; McMeeking, G.R.; Seinfeld, J.H.; Soni, T.; Taylor, J.W.; Weise, D.R.; Wold, C.E. Investigating the links between ozone and organic aerosol chemistry in a biomass burning plume from a prescribed fire in California chaparral. *Atmos. Chem. Phys.* **2015**, *15*, 6667–6688.

Bell, M. L., McDermott, A., Zeger, S. L., Samet, J. M., & Dominici, F. Ozone and short-term mortality in 95 US urban communities, 1987-2000. *JAMA*, *292*(19), 2372–2378. https://doi.org/10.1001/jama.292.19.2372, 2004.

Bernays, N., Jaffe, D. A., Petropavlovskikh, I., and Effertz, P.: Comment on "Comparison of ozone measurement methods in biomass burning smoke: an evaluation under field and laboratory conditions" by Long et al., Atmos. Meas. Tech., 15, 3189–3192, https://doi.org/10.5194/amt-15-3189-2022, 2022.

Birks, J. W., Andersen, P. C., Williford, C. J., Turnipseed, A. A., Strunk, S. E., Ennis, C. A., & Mattson, E. (2018). Folded tubular photometer for atmospheric measurements of NO_2 and NO. *Atmospheric Measurement Techniques*, 11, 2821– 2835. https://doi.org/10.5194/amt-11-2821-2018

Buysse, C.E., Kaulfus, A., Nair, U., and Jaffe D.A.: 2019. Relationships between particulate matter, ozone, and nitrogen oxides during urban smoke events in the western US. Environ Sci Technol 53, 21, 12519-12528, doi: 10.1021/acs.est.9b05241.

Coggon, M.M.; Lim, C.Y.; Koss, A.R.; Sekimoto, K.; Yuan, B.; Gilman, J.B.; Hagan, D.H.; Selimovic, V.; Zarzana, K.J.; Brown, S.S.; Roberts, J.M.; Müller, M.; Yokelson, R.; Wisthaler, A.; Krechmer, J.E.; Jimenez, J.L.; Cappa, C.; Kroll, J.H.; de Gouw, J.; Warneke, C. OH chemistry of non-methane organic gases (NMOGs) emitted from laboratory and ambient biomass burning smoke: evaluating the influence of furans and oxygenated aromatics on ozone and secondary NMOG formation. *Atmos. Chem. Phys.* **2019**, *19*, 14875–14899.

Di, Q., Dai, L. Z., Wang, Y., Zanobetti, A., Choirat, C., Schwartz, J. D., & Dominici, F. Association of short-term exposure to air pollution with mortality in older adults. Journal of the American Medical Association, 318(24), 2446–2456. https://doi.org/10.1001/jama.2017.17923, 2017.

Gong X., A. Kaulfus, U. Nair and D. A. Jaffe, Quantifying O_3 Impacts in Urban Areas Due to Wildfires Using a Generalized Additive Model, Environmental Science and Technology, 2017, **51 (22)**, 13216–13223. https://doi.org/10.1021/acs.est.7b03130.

Ho, S. S. H., Ip, H. S. S., Ho, K. F., Dai, W.-T., Cao, J., and Ng, L. P. T.: concerns on the use of ozone scrubbers for gaseous carbonyl measurement by DNPH-coated silica gel cartridge, *Aerosol Air Qual. Res.*, **2013**, 13, 1151-1160.

Hu, L., Millet, D.B., Kim, S.Y., Wells, K.C., Griffiths, T., Fischer, E., Helmig, D. Hueber, J., and Curtis, A., North American acetone sources determined from tall tower measurements and inverse modeling, *Atmos. Chem. Phys.* **2013,** 13, 3379-3392.

Jacob, D.J. Heterogeneous chemistry and tropospheric ozone. *Atmos. Environ.* **2000**, *34*, 2131–2159.

Jaffe D.A., Fiore A.M. and Keating, T.J. Importance of Background O_3 for Air Quality Management. EM. November 2020.

Jaffe D. Evaluation of Ozone Patterns and Trends in 8 Major Metropolitan Areas in the U.S. Final project report for CRC Project A-124, Coordinating Research Council, Alpharetta, GA, March 2021. Available at: http://crcao.org/wp-content/uploads/2021/04/CRC-Project-A-124-Final-Report_Mar2021.pdf

Jenkin, M.E.; Young, J.C.; Rickard, A.R. The MCM v3.3.1 degradation scheme for isoprene. *Atmos. Chem. Phys.* **2015**, *15*, 11433–11459.

Kaulfus, A.S., Nair, U., Jaffe, D.A., Christopher, S.A., and Goodrick, S.. Biomass burning smoke climatology of the United States: Implications for particulate matter air quality, Environmental Science & Technology 50, 11731-11741, doi: 10.1021/acs.est.7b03292, 2017.

Langford, A. O., Alvarez, R. J., II, Brioude, J., Fine, R., Gustin, M. S., Lin, M. Y., et al. Entrainment of stratospheric air and Asian pollution by the convective boundary layer in the southwestern U.S. Journal of Geophysical Research: Atmospheres, 122, 1312–1337. https://doi.org/10.1002/2016JD025987, 2017.

Lindsay, A.J.; Anderson, D.C.; Wernis, R.A.; Liang, Y.; Goldstein, A.H.; Herndon, S.C.; Roscioli, J.R.; Dyroff, C.; Fortner, E.C.; Croteau, P.L.; Majluf, F.; Krechmer, J.E.; Yacovitch, T.I.; Knighton, W.B.; Wood, E.C. Ground-based investigation of HO_x and ozone chemistry in biomass burning plumes in rural Idaho. *Atmos. Chem. Phys.* **2022**, *22*, 4909–4928.

Long, R. W., Whitehill, A., Habel, A., Urbanski, S., Halliday, H., Colón, M., Kaushik, S., and Landis, M. S., 2021. Comparison of ozone measurement methods in biomass burning smoke: an evaluation under field and laboratory conditions, Atmos. Meas. Tech., 14, 1783–1800, https://doi.org/10.5194/amt-14-1783-2021.

Louisiana Department of Environmental Quality (LDEQ), 2018. Louisiana Exceptional Event of September 14, 2017: Analysis of Atmospheric Processes Associated with the Ozone Exceedance

and Supporting Data. Available at https://www.epa.gov/sites/production/files/2018-08/documents/ldeq_ee_demonstration_final_w_appendices.pdf.

Lyman, S. N., Holmes, M., Tran, H., Tran, T., and O'Neil, T.: High ethylene and propylene in an area dominated by oil production, *Atmosphere* **2021**, 12, 1.

Mason, S.A.; Trentmann, J.; Winterrath, T.; Yokelson, R.J.; Christian, T.J.; Carlson, L.J.; Warner, T.R.; Wolfe, L.C.; Andreae, M.O. Intercomparison of Two Box Models of the Chemical Evolution in Biomass-Burning Smoke Plumes. *J. Atmos. Chem.* **2006**, *55*, 273–297.

Mathur, R., Kang, D., Napelenok, S. L., Xing, J., Hogrefe, C., Sarwar, G., et al. (2022). How have divergent global emission trends influenced long-range transported ozone to North America? Journal of Geophysical Research: Atmospheres, 127, e2022JD036926. https://doi.org/10.1029/2022JD036926.

McClure C.D. and Jaffe D.A. Investigation of High Ozone Events due to Wildfire Smoke in an Urban Area. Atmos. Envir. https://doi.org/10.1016/j.atmosenv.2018.09.021, 2018.

McDuffie, E.E.; Edwards, P.M.; Gilman, J.B.; Lerner, B.M.; Dubé, W.P.; Trainer, M.; Wolfe, D.E.; Angevine, W.M.; deGouw, J.; Williams, E.J.; Tevlin, A.G.; Murphy, J.G.; Fischer, E.V.; McKeen, S.; Ryerson, T.B.; Peischl, J.; Holloway, J.S.; Aikin, K.; Langford, A.O.; Senff, C.J.; Alvarez II, R.J.; Hall, S.R.; Ullmann, K.; Lantz, K.O.; Brown, S.S. Influence of oil and gas emissions on summertime ozone in the Colorado Northern Front Range. *J. Geophys. Res.: Atmos.* **2016**, *121*, 8712–8729.

Müller, M.; Anderson, B.E.; Beyersdorf, A.J.; Crawford, J.H.; Diskin, G.S.; Eichler, P.; Fried, A.; Keutsch, F.N.; Mikoviny, T.; Thornhill, K.L.; Walega, J.G.; Weinheimer, A.J.; Yang, M.; Yokelson, R.J.; Wisthaler, A. In situ measurements and modeling of reactive trace gases in a small biomass burning plume. *Atmos. Chem. Phys.* **2016**, *16*, 3813–3824.

Ninneman, M.; Jaffe, D.A. The impact of wildfire smoke on ozone production in an urban area: Insights from field observations and photochemical box modeling. *Atmos. Environ.* **2021**, *267*, 118764.

Ninneman, M.; Lu, S.; Zhou, X.; Schwab, J. On the Importance of Surface-Enhanced Renoxification as an Oxides of Nitrogen Source in Rural and Urban New York State. *ACS Earth Space Chem.* **2020**, *4*, 1985–1992.

Norris, G., Duvall, R., Brown S., Bai, S., EPA Positive Matrix Factorization (PMF) 5.0 Fundamentals and User Guide. **2023**, https://www.epa.gov/sites/default/files/2015-02/documents/pmf_5.0_user_guide.pdf.

Paatero, P., Tapper, U., "Positive matrix factorization: A non-negative factor model with optimal utilization of error estimates of data values, *Environmetrics* **1994**, 5, 111-126.

Permar, W., L. Jin, Q. Peng, K. O'Dell, E. Lill, V. Selimovic, R. J. Yokelson, R. S. Hornbrook, A. J. Hills, E. C. Apel, I-T. Ku, Y. Zhou, B. C. Sive, A. P. Sullivan, J. L. Collett Jr., B. B. Palm, J. A. Thornton, F. Flocke, E. V. Fischer, L. Hu, Atmospheric OH reactivity in the western United States determined from comprehensive gas-phase measurements during WE-CAN, *Environ. sci.: Atmos*., **2023**, https://doi.org/10.1039/D2EA00063F.

Rickly, P.S.; Coggon, M.M.; Aikin, K.C.; Alvarez II, R.J.; Baidar, S.; Gilman, J.B.; Gkatzelis, G.I.; Harkins, C.; He, J.; Lamplugh, A.; Langford, A.O.; McDonald, B.C.; Peischl, J.; Robinson, M.A.; Rollins, A.W.; Schwantes, R.H.; Senff, C.J.; Warneke, C.; Brown, S.S. Influence of Wildfire on Urban Ozone: An Observationally Constrained Box Modeling Study at a Site in the Colorado Front Range. *Environ. Sci. Technol.* **2023**, *57*, 1257–1267.

Rolph, G. D.; Draxler, R. R.; Stein, A. F.; Taylor, A.; Ruminski, M. G.; Kondragunta, S.; Zeng, J.; Huang, H.-C.; Manikin, G.; Mcqueen, J. T.; et al. Description and Verification of the NOAA Smoke Forecasting System: The 2007 Fire Season. Weather Forecast., 24, 361−378, 2009.

Sekimoto, K.; Li, S.-M.; Yuan, B.; Koss, A.; Coggon, M.; Warneke, C.; de Gouw, J. Calculation of the Sensitivity of Proton-Transfer-Reaction Mass Spectrometry (PTR-MS) for Organic Trace Gases Using Molecular Properties. *International Journal of Mass Spectrometry* **2017**, *421*, 71–94. https://doi.org/10.1016/j.ijms.2017.04.006.

Slade, J.H.; Knopf, D.A. Multiphase OH oxidation kinetics of organic aerosol: The role of particle phase state and relative humidity. *Geophys. Res. Lett.* **2014**, *41*, 5297–5306.

Tang, M.J.; Cox, R.A.; Kalberer, M. Compilation and evaluation of gas phase diffusion coefficients of reactive trace gases in the atmosphere: volume 1. Inorganic compounds. *Atmos. Chem. Phys.* **2014**, *14*, 9233–9247.

Texas Commission of the Environment (TCEQ), 2017. El Paso Ozone Exceptional Event: June 21, 2015, Addendum 4: Update, May 17, 2017.

Trebs, I.; Bohn, B.; Ammann, C.; Rummel, U.; Blumthaler, M.; Königstedt, R.; Meixner, F.X.; Fan, S.; Andreae, M.O. Relationship between the NO_2 photolysis frequency and the solar global irradiance. *Atmos. Meas. Tech.* **2009**, *2*, 725–739.

U.S. EPA, "Guidance on the Preparation of Exceptional Events Demonstrations for Wildfire Events that May Influence Ozone Concentrations", 2015. Retrieved from: https://www.epa.gov/sites/production/files/2015-11/documents/o3_draft_wildfire_guidance.pdf.

Vlasenko, A., Macdonald, A., Sjostedt, S., and Abbatt, J.: Formaldehyde measurements by Proton transfer reaction–Mass Spectrometry (PTR-MS): correction for humidity effects, *Atmos. Meas. Tech.* **2010**, 3, 1055-1062.

Walker S.E., S. Solberg, P. Schneider and C. Guerreiro, The AirGAM 2022r1 air quality trend and prediction model, Geoscientific Model Development, 2023, **16**, 573–595. https://doi.org/10.5194/gmd-16-573-2023.

Wolfe, G.M., Marvin, M.R., Roberts, S.J., Travis, K.R., Liao, J., 2016. The Framework for 0-D atmospheric modeling (F0AM) v3.1. Geosci. Model Dev 9, 3309–3319. https://doi.org/10.5194/gmd-9-3309-2016.